Check for updates

Generation of nanoscopic membrane curvature for membrane trafficking

Michael M. Kozlov[1] ✉ *and Justin W. Taraska*[2] ✉

Abstract | Curved membranes are key features of intracellular organelles, and their generation involves dynamic protein complexes. Here we describe the fundamental mechanisms such as the hydrophobic insertion, scaffolding and crowding mechanisms these proteins use to produce membrane curvatures and complex shapes required to form intracellular organelles and vesicular structures involved in endocytosis and secretion. For each mechanism, we discuss its cellular functions as well as the underlying physical principles and the specific membrane properties required for the mechanism to be feasible. We propose that the integration of individual mechanisms into a highly controlled, robust process of curvature generation often relies on the assembly of proteins into coats. How cells unify and organize the curvature-generating factors at the nanoscale is presented for three ubiquitous coats central for membrane trafficking in eukaryotes: clathrin-coated pits, caveolae, and COPI and COPII coats. The emerging theme is that these coats arrange and coordinate curvature-generating factors in time and space to dynamically shape membranes to accomplish membrane trafficking within cells.

Caveolae
Flask-shaped nano-structures of plasma membrane rich in proteins, as well as lipids such as cholesterol and sphingolipids, and having several functions in intracellular signal transduction.

Phagophore
A flat cisterna-like membrane compartment serving as a precursor of autophagosome formation.

Mitochondrial cristae
Folds in the inner membrane of a mitochondrion.

[1]*Department of Physiology and Pharmacology, Sackler Faculty of Medicine, Tel Aviv University, Tel Aviv, Israel.*

[2]*Biochemistry and Biophysics Center, National Heart, Lung, and Blood Institute, National Institutes of Health, Bethesda, MD, USA.*

✉*e-mail:* *michk@tauex.tau.ac.il*; *justin.taraska@nih.gov*

https://doi.org/10.1038/s41580-022-00511-9

Cellular membranes compartmentalize the complex chemistry of life. These compartments are created by the cell in a remarkably diverse set of shapes, which are dynamic, and in many cases topologically complex (FIG. 1). Examples include convoluted and persistently transforming membrane structures appearing on the plasma membrane of eukaryotic cells, which include the budding intermediates of various endocytic mechanisms[1], clusters of caveolae[2–4] and T-tubular networks of muscle cells[5,6]. Deeper in the cell, intricate shapes and topologies characterize the extended[7,8] and nanoscopic[9] networks of peripheral endoplasmic reticulum (ER) and the associated ER exit sites[10] (FIG. 1), the stacks of unevenly perforated cisternae of the Golgi complex interconnected into bands by networks of tubules[11], the inner membranes of mitochondria[12,13], membranes of thylakoids in chloroplasts[14] and the pleomorphic post-Golgi membrane carriers[15] made of clusters of interconnected spherical buds. All these systems form the underlying membrane networks needed to produce secreted proteins, activate signalling complexes, move material across the cell, internalize material and coordinate the complex metabolism of cells and organisms.

Although the architecture of each of the membrane systems is unique, it is generated from a limited palette of shape elements and, therefore, configurations of different systems must rely on a common set of physical mechanisms. These shape elements are spheres, cylinders, disc-like cisternae and the membrane junctions between them[16]. Recent theoretical work suggested that non-axisymmetric membrane shapes appearing as deformed spheres may form under certain conditions whose relevance for intracellular membranes is yet to be demonstrated[17–19].

While exhibiting different configurations, these shape elements share a prominent geometric feature — significant membrane curvatures (see[16] for curvature definitions). What is the scale of this curvature? All membrane building blocks have cross-sectional radii of curvature in the nanoscopic range between a few tens of nanometres and a few hundred nanometres. Spheres of this radii are typical for most intracellular and extracellular vesicles and buds[20–22]. Shapes of smooth or irregular cylinders of 30–100-nm cross-sectional radii characterize such structures as tubules of the peripheral ER[23], T-tubular extensions of plasma membranes[5], fragments of non-spherical transport intermediates, elements of tubular networks of Golgi ribbons[15] and protrusions of plasma membrane forming in the processes of cell spreading on and movement along extracellular substrate, which include filopodia[24] and retraction fibers[25]. The disc-like cisterna shapes characterizing the sheets of rough ER of mammalian cells[26] and thylakoidal membranes of plant cells[14], the phagophore structures during autophagy[27], the cisternae of Golgi stacks[15] and the mitochondrial cristae[12,13] consist of nearly flat and mutually parallel top and bottom membranes connected by a strongly curved membrane of the disc rim with cross-sectional radii in the 20–50-nm range.

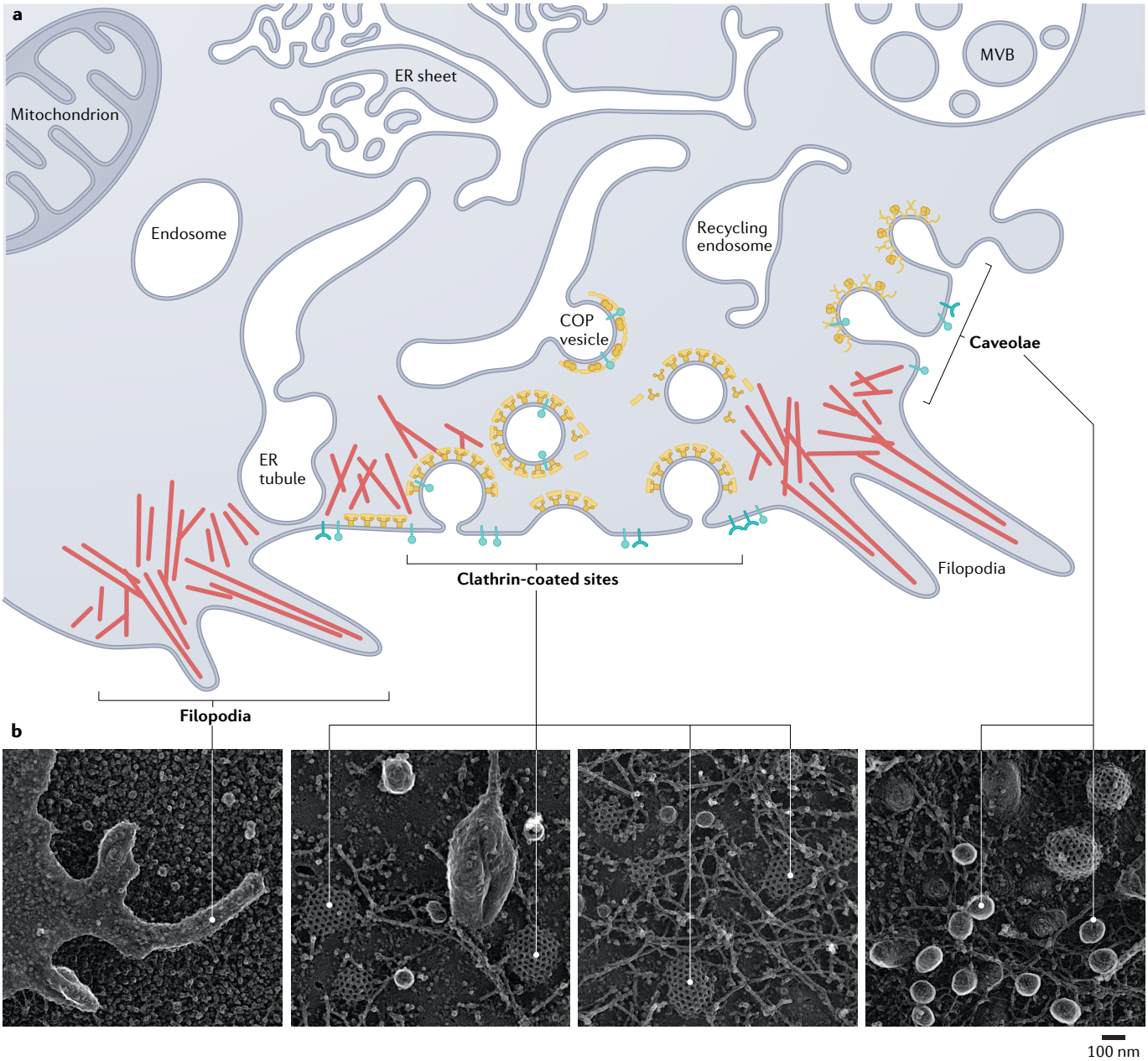

Fig. 1 | **Complexity of intracellular membrane shapes. a** | Schematic representation of the cell interior highlighting multiple curved membrane structures. **b** | Examples of curved membranes in cells visualized by electron microscopy. The leftmost image shows membrane extensions on the outside of a mammalian HeLa cell. The three images to the right show platinum replica electron microscopy images of different complex shapes at the inner plasma membrane of U87 and HeLa cell plasma membranes: clathrin-coated pits, caveolae and other near-plasma-membrane structures can be seen. ER, endoplasmic reticulum; MVB, multivesicular body. Images are courtesy of Kem Sochacki and Bijeta Prasai (Taraska laboratory, NHLBI).

The geometry of membrane junctions is qualitatively different from that of the spheres, cylinders and discs. While the latter have convex shapes, junctional membranes are saddle-like (that is, simultaneously convex and concave). These include hourglass-like junctions connecting endocytic buds[28] and caveolar bulbs[29] to the plasma membrane and to each other[2,30], the three-way junctions between ER tubules[31], the helicoidal junctions between ER sheets[26] and the T-junctions between the ER tubules and sheets[32]. However, the junctions have the same tens of nanometre range of cross-sectional radii of curvature.

While the basic geometric features of membrane shape elements are known, fundamental gaps in our understanding of the mechanisms of their formation remain. In this Review, we focus on the mechanisms of nanoscale curvature generation and their relationship to protein coats used for intracellular trafficking in eukaryotes.

Mechanisms of curvature generation

Membrane curvature is considered to be large if the cross-sectional radius of the membrane surface is comparable to the membrane thickness of about 5 nm, and

small otherwise. Typical elements of intracellular membranous compartments can have cross-sectional radii of about 20 nm and, hence, are characterized by large curvatures. The creation of some membrane curvature is, generally, an 'easy' task since curving is a common result of any trans-bilayer asymmetry found in the membrane structure[33] or differences between the separated aqueous environments[34] (cytosol versus bodily fluids, for example). However, the generation of large curvatures such as those of intracellular membranes requires special conditions providing strong curvature-generating factors. These conditions can be provided by external forces applied to the membrane[35], phase separation of lipids in the membrane plane resulting in nanodomains/microdomains[36], asymmetric ionic conditions[37] in the surrounding solutions, asymmetric lipid composition of the leaflets[16] and proteins that bind to or penetrate one of the leaflets. While many reviews have discussed the basic physical mechanisms of membrane bending (for recent developments, see[38]), current advances in our understanding of the complex biological processes that use membrane shaping such as clathrin-mediated endocytosis inside living cells have provided new insights into the level of complexity and the mechanisms exploited by cells to locally curve their membranes in a manner that can be regulated in time and space.

Here we specifically concentrate on the mechanisms of membrane bending induced by proteins, which are most common in intracellular membrane dynamics. To gain a global systematic view, we first discuss the basic mechanisms, each originating from a different mode of interactions between a protein and the lipid bilayer. These basic mechanisms can be subdivided into two types. First, those driven by a direct interaction of a protein domain with the bilayer core. These include the hydrophobic insertion (or wedging) mechanism[39,40]. Second, mechanisms in which the curvature-generating forces are applied externally to the bilayer surface by the extra-bilayer protein domains. Here, the bilayer core remains intact. These encompass crowding[41] and scaffolding[42] mechanisms.

We synthesize the emergent mechanisms into more complex ones that require coordination between the basic modes. We do not address the roles played in the membrane curvature generation and shaping by the membrane lipid composition[33,43,44] and the lateral tension[45], the mechanical stress generated in the membrane by stretching forces applied to the membrane surface by the cytoskeleton or osmotic pressure. These important and broad topics deserve separate discussions, which are beyond the scope of the present Review.

Hydrophobic insertion mechanism

The hydrophobic insertion — wedging — mechanism of membrane curving is used by a large group of diverse proteins having a common feature — one or several amphipathic or hydrophobic domains. Embedding of these domains to some degree into the hydrophobic core of a lipid monolayer creates a local structural asymmetry which causes bending[40,46–50]. Membrane bending has a directionality and, therefore, curvature can be either positive or negative[51]. Here and later, we use the common convention[16], where positive curvature corresponds to a lipid monolayer or bilayer bulging in the direction of the surface exposed to the curvature-generating proteins, and negative curvature corresponds to a lipid monolayer or bilayer bulging in the opposite direction. A positive curvature induced in one monolayer causes a positive curvature of the whole bilayer since the two membrane monolayers are held together by the hydrophobic interaction[39,40,49]. Specifically, hydrophobic insertions generate a positive curvature of lipid monolayers and, hence, of bilayers.

Phenomenology

The protein domains commonly proposed to use the hydrophobic insertion mechanism are amphipathic helices, small hydrophobic loops and asymmetric oligomers of hydrophobic hairpins.

Amphipathic helices are short protein sequences, which have, or acquire upon interaction with a lipid bilayer, helical structures with a common feature — the nonpolar and polar residues are aligned along the opposite faces of the helix[52–54]. Interactions of the nonpolar face of this helix with the hydrophobic core of the membrane drives a shallow insertion of the domain into the membrane[55]. Typically, amphipathic helix embedding depth reaches the interface between the polar heads and hydrophobic tails within the monolayer[56–59], but can vary[56,60]. The role of amphipathic helix insertion in generating membrane curvature has been the subject of much work over decades[33,38,52,55]. Experimentally, the ability to generate large curvatures was demonstrated for amphipathic helix-containing domains from a number of proteins involved in a plethora of intracellular processes (see TABLE 1). A related mechanism is membrane curvature generation by small hydrophobic loops, which penetrate one leaflet to the depth of lipid's glycerol backbones[61,62] (TABLE 1).

Likewise, the generation of membrane curvature by hydrophobic hairpins has been demonstrated for transmembrane domains of receptor expression-enhancing proteins (REEPs). These proteins assemble into dimers whose hairpins were proposed to have a strongly splayed configuration of an effective inverted cone-like shape[63]. Tilting of the hydrocarbon chains of lipid molecules adjacent to such an inverted cone results in a large local curvature of the surrounding membrane[63].

Qualitative physics of the mechanism

The hydrophobic insertion mechanism works by creating a local deformation of tilt and splay (BOX 1) in the lipid hydrocarbon chains[40,64–67]. To alleviate the energy of the emerging stresses, the monolayer deviates from the initial flat shape, acquiring a local curvature[40] (FIG. 2a, left). The insertions generate curvature only locally, generally within a few nanometres around the embedded protein domains. The exact dimensions of this region are set by the size of the inserted protein region and hence the size of the insertion, and by the length to which the tilt and splay propagate along the plane of the membrane[68]. The sizes of the typical amphipathic helices, such as those of the ENTH domain, N-BAR domains and the small GTPases SAR1 and ARF1, as well as the sizes of C2 domain small

Receptor expression-enhancing proteins
(REEPs). Proteins belonging to the Yip (Ypt-interacting protein) family and identified by their ability to enhance cell surface expression of a subset of G protein-coupled receptors.

ENTH domain
The epsin amino-terminal homology domain serving as a structural domain that is found in proteins involved in endocytosis and cytoskeletal machinery.

BAR domains
Highly conserved protein dimerization domains that occur in many proteins involved in membrane dynamics in a cell. BAR domains are named after three proteins that they are found in: BIN, amphiphysin and Rvs.

SAR1
A protein involved in membrane trafficking. It is a monomeric small GTPase found in COPII vesicles.

ARF1
ADP-ribosylation factor involved in protein trafficking among different compartments. It modulates vesicle budding and uncoating within the Golgi complex.

Table 1 | **Proteins using the hydrophobic insertion mechanism**

Protein	Function	Refs.
Amphipathic helices		
ENTH domains of epsins	Components of clathrin coat-mediated membrane budding	39,199–202
ANTH domains of CALM	Components of clathrin coat-mediated membrane budding	83
Synucleins	The presynaptic membrane-binding proteins implicated in the pathogenesis of Parkinson disease	203–207
Apolipoprotein A-1	Lipid metabolism	60
Peptides corresponding to the amphipathic helix of wild type Yop1	Curving tubules and sheet edges of the peripheral endoplasmic reticulum	63,208
Peptides corresponding to the amphipathic helix of REEP	Curving tubules and sheet edges of the peripheral endoplasmic reticulum	63,208
Amphipathic helix peptide of Pex11	In peroxisome proliferation	209,210
Small GTPase SAR1	Regulation of the assembly on endoplasmic reticulum membranes of COPII coats	196,211,212
Small GTPase ARF1	Formation of COPI coats on Golgi complex membranes	197,213,214
Influenza virus M2	Multifunctional protein with proton-selective ion channel activity implicated in membrane scission	215
N-BAR family proteins	Endocytic membrane budding	57,216–219
Small hydrophobic loops		
C2A and C2B domains of synaptotagmin 1	Ca^{2+} sensor of the SNARE-mediated membrane fusion machinery	71,220
DOC2B	Widely expressed in nerve terminals and interacting with SNARE components	221,222
Hydrophobic hairpins		
REEP dimers	Curving tubules and sheet edges of the peripheral endoplasmic reticulum	63,208

REEP, receptor expression-enhancing protein.

hydrophobic loops and of the splayed hairpin dimers of REEPs are all in the few nanometre range. Also, the characteristic length of tilt and splay propagation is only a few nanometres (BOX 1).

The value of local curvature produced by a hydrophobic insertion depends on the degree of monolayer asymmetry generated. For amphipathic helices and small hydrophobic loops, the asymmetry depends mostly on the insertion depth[40,47,69], which may differ between tubular and spherical membranes[56,70]. On one hand, a bound but not yet embedded domain, for all practical purposes, does not perturb the monolayer structure and, hence, produces no to little asymmetry (FIG. 2a, top). On the other hand, if an insertion penetrates as deeply as the middle of the monolayer, the monolayer structure becomes disturbed but in a symmetric fashion, which does not result in curvature (FIG. 2a, right). The maximal curvature was predicted to be generated by hydrophobic insertions reaching the interface between the polar heads and the hydrocarbon tails of lipid molecules; that is, penetrating about a third of the monolayer thickness[40] (FIG. 2a, left). The insertion depth corresponding to the maximal curvature is referred to later as the 'optimal depth'.

Synaptotagmin
A family of proteins with an amino-terminal transmembrane domain and two cytoplasmic C2 domains. Many C2 domains mediate calcium-dependent binding to negatively charged membranes.

Lysolipids
Any derivative of a lipid in which one hydrocarbon chain has been removed by hydrolysis.

According to this prediction, and the experimental results on insertion depths[56,57,59], amphipathic helices are the most effective curvature generators.

The ability of an insertion to generate membrane curvature can be quantified by the insertion's effective intrinsic curvature, ζ, which characterizes the curvature of a particle consisting of the insertion itself and a limited number of the adjacent lipid molecules subjected to the insertion-related strains and stresses (FIG. 2a, bottom left). The practical meaning of ζ is the curvature of a monolayer that consists solely of the effective particles and is not subject to any forces or constraints. Hydrophobic insertions characterized by larger ζ values have a stronger potential to generate membrane curvature. The estimated values of the intrinsic curvatures of several hydrophobic insertions are about 1 nm^{-1} for amphipathic helices embedded to the optimal depth[40,69], and about 0.7 nm^{-1} for the C2AB domain of synaptotagmin[71]. These values can be compared with the intrinsic curvatures of the so-called non-bilayer lipids involved in modulation of membrane remodelling by fusion and fission[72]. The most efficient generators of positive spontaneous curvature are lysolipids, whose molecular intrinsic curvatures lie in the range between about 0.26 nm^{-1} and about 0.15 nm^{-1} (REF.[73]). Hence, amphipathic helices appear to be the most powerful among the currently characterized producers of positive monolayer curvature.

It must be noted, however, that the value of the effective intrinsic curvature of a protein insertion may be influenced by the intrinsic curvatures of lipid molecules adjacent to it.

Reservations concerning the mechanism

The ability of hydrophobic insertions to generate membrane curvature has been questioned by several experimental studies in which amphipathic helices were embedded in the membrane either as separate peptides[74] or in the context of N-BAR domains[75] and were shown to produce no measurable curvature. These observations are, likely, a consequence of a rather strong sensitivity of generated curvature to the depth of amphipathic helix insertion[40,47]. Even subtle deviations of the insertion depth from the optimal values have been predicted to result in a substantial reduction in curvature[40]. The presence of the BAR domain was shown to shift the amphipathic helix of the N-BAR domain deeper than the optimal position[59]. Also, synthetic peptides corresponding to amphipathic helices of N-BAR domains used previously[74] apparently underwent a too-deep insertion. Hence, in both cases, the reason for a weak or effectively absent effect on curvature was likely due to excessive insertion depths of the domains.

Leaflet expansion effect

In addition to producing local membrane curvature, embedded protein domains contribute to another mode of curvature generation, which is unrelated to the induction of monolayer structural asymmetry. This mechanism is based solely on the increase of the area of the insertion-containing monolayer due to the added area of the insertions, as compared with the area of the second membrane monolayer, which remains insertion-free.

Helfrich model
A theoretical model describing the bending elasticity of lipid membranes. It enables computations of the energy of membrane curvature generation and is based on the concepts of membrane spontaneous curvature and bending moduli.

Epsins
A family of highly conserved membrane proteins that are important in creating membrane curvature. Epsins contribute to membrane deformations like endocytosis, and block vesicle formation during mitosis.

CALM
Clathrin assembly lymphoid myeloid, a member of ANTH-domain containing proteins that promotes clathrin assembly.

The difference in the monolayer areas drives membrane bending, which is referred to as the 'bilayer-couple mechanism'[76]. The bilayer-couple mechanism, which may be modulated by a difference of the monolayer lipid compositions[77,78], is sometimes considered to be the major (or even singular) effect of hydrophobic insertions (see[52], for example). Importantly, this mechanism, has a global rather than a local character since the curvature it generates is determined by the difference between the total areas of the two membrane monolayers. Thus, the contribution of each insertion is averaged over the entire membrane surface. This challenges the relevance of this effect for most intracellular processes. For example, in endocytic vesicles, proteins are inserted only locally within the tens of nanometre-sized budding region such that their contribution to the overall area of a few tens of square microns of the plasma membrane monolayer is vanishingly small. As a result, the curvature generated by the bilayer-couple mechanism must be, for all practical purposes, negligible. By contrast, the mechanism based on local structural asymmetry provides curvature directly to the location of the protein insertion itself, and its effects are independent of the surrounding membrane. We thus support a model where this local mechanism is dominant in shaping organelles and transport intermediates.

Multiple hydrophobic insertions

Because an inserted protein generates curvature only in its close vicinity, producing curvature along extended areas requires enrichment of these regions in multiple insertion points (FIG. 2b). The contribution of multiple hydrophobic insertions to the energetically preferable curvature of a large-scale area, J_m, depends on the area fraction, ϕ, the insertions occupy in the monolayer plane and on the effective intrinsic curvature of each insertion, ζ. J_m can be, approximately, presented as $J_m = \phi\zeta$ (REFS.[79,80]). The related contribution to the preferable curvature of a bilayer whose second monolayer does not contain the hydrophobic insertions is given by $J_b = \frac{1}{2}\phi\zeta$. On this basis, the generation of a spherical membrane with 70-nm radius corresponding, approximately, to that of an endocytic vesicle would require about 6% area coverage ($\phi \approx 0.06$) by the amphipathic helices with $\zeta \approx 1\,\mathrm{nm}^{-1}$.

Importantly, an enrichment of a membrane region in hydrophobic insertions up to a certain area fraction, ϕ, requires work performed by direct or indirect forces acting on the insertions and counteracting two key factors that resist this enrichment. One factor is the entropy of the insertion distribution in the membrane plane, which disfavours large insertion concentrations. The related energy cost of the insertion enrichment is on the order of the thermal energy, $k_BT \approx 0.6\,\mathrm{kcal\,mol^{-1}}$ per insertion. The second factor is a membrane-mediated repulsion predicted to develop between the insertions because of the tilt and splay deformations (BOX 1) they induce in the surrounding membrane[81]. The energy of this repulsion (BOX 1) per insertion of a few nanometres in length can be estimated to have a typical value of a few k_BT. For the insertional enrichment, the repulsive forces and the entropy must be counteracted by factors working to concentrate the insertions within dedicated regions in the membrane plane. The most likely source of these concentrating forces is a direct or indirect binding of the proteins to each other or to other protein structures (that is, coats). An example of the latter is the recruitment of epsins[82] and CALM[83] to the clathrin lattice during endocytosis.

Protein crowding mechanisms

Membrane curvature generation by protein crowding was initially proposed for a specific mode of membrane bending driven by collisions of proteins attached to and freely moving along the membrane surface[41]. However, it can be generalized to a family of mechanisms in which membrane curvature originates from nonspecific and concentration-dependent interactions between hydrophilic proteins associated with the membrane surface. Two types of interactions are thought to contribute to the crowding mechanisms: (1) interactions mediated by entropy and (2) generic electrostatic or multivalent interactions. We discuss each in the following subsections.

Entropic interaction mechanisms

The entropic forces fuelling the crowding mechanisms can originate either from the collective entropy of protein distributions along the plane of the membrane or from internal entropy (disorder) of the individual proteins themselves.

The distribution entropy mechanism initially aimed at explaining the generation of large membrane curvatures by several proteins and hydrophilic domains of proteins involved in endocytosis, such as

Box 1 | Deformations and elastic energies of tilt and splay

Modelling of the hydrophobic insertion mechanism of curvature generation requires consideration of intra-monolayer deformations of tilt and splay of the hydrocarbon chains of lipid molecules[64–67] (see the figure), which are not accounted for by the common Helfrich model of membrane elasticity[223]. The tilt deformation, $\vec{t}$, is the deviation of the average direction of the hydrocarbon chains, $\vec{d}$, from the normal to the monolayer surface, $\vec{N}$, so $\vec{t} = \vec{d} - \vec{N}$ (see the figure, middle part). The splay deformation originates from the variation of the tilt along the surface, and is defined as the surface divergence of the tilt, $\nabla\vec{t}$ (REF.[66]) (see the figure, right part). The energies of these deformations are set by the elastic moduli of tilt, κ_t, splay, κ, and saddle splay, $\bar{\kappa}$ (REFS.[224–226]). The values of the elastic moduli of splay, κ, and tilt, κ_t, are positive, while the saddle splay modulus was found to be negative[227].

The tilt and splay elasticities of lipid monolayers set the extent of curvatures generated by hydrophobic insertions[40] and determine the energies of intermediate structures of membrane fusion and fission[228,229].

The characteristic length of propagation of the tilt-related deformations along the membrane plane, λ_d, is determined by the ratio of the elastic moduli, $\lambda_d \approx \sqrt{\frac{\kappa}{\kappa_t}}$. If one takes into account that κ_t ranges between 20 mN m^{-1} and 80 mN m^{-1} (REFS.[224–226]) and κ is about $10k_BT$ (where $k_BT \approx 4\times10^{-21}$ Joule)[230], λ_d typically has values in the 1–3-nm range.

The elastic energy of tilt and splay enables, for example, evaluation of the energy needed to bring together two rod-like insertions, which model amphipathic helices of various proteins[52–54]. This energy needed to overcome the mutual repulsion mediated by the tilt and splay deformations the insertions generate in the membrane can be estimated according to $\sqrt{\kappa_m\kappa_t}\,l$, where l is the insertion length.

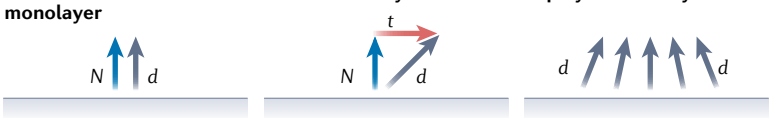

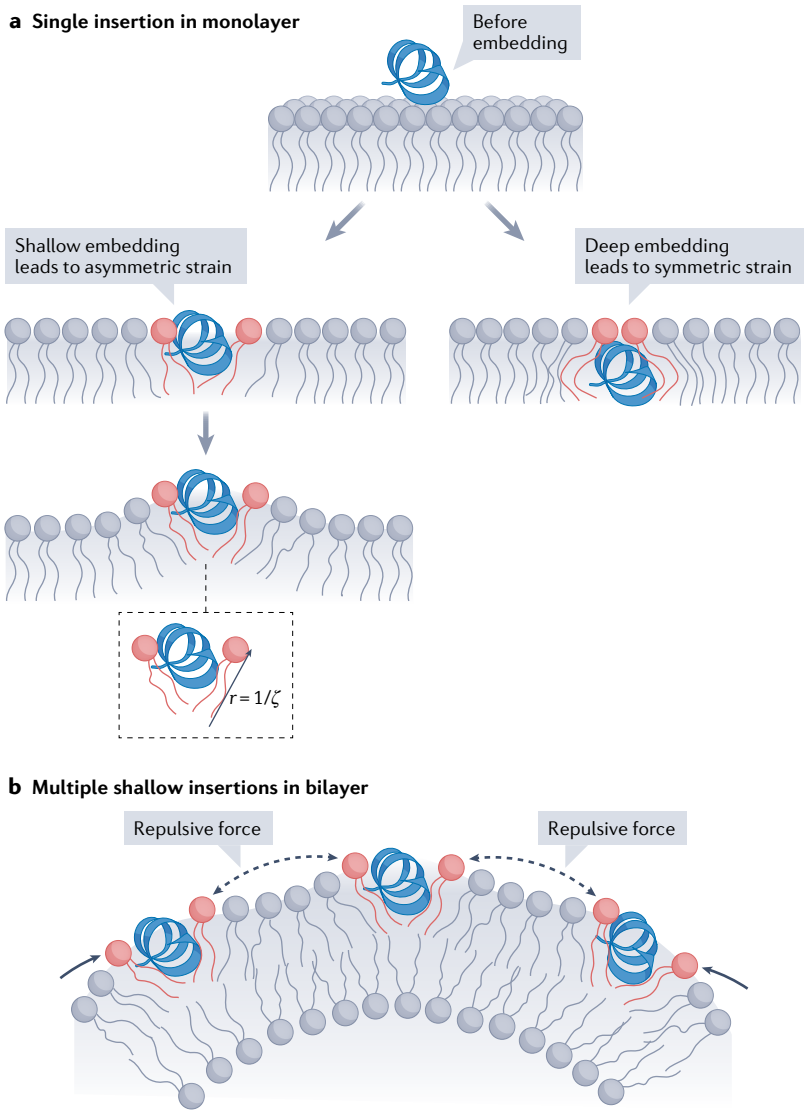
a Single insertion in monolayer
Before embedding
Shallow embedding leads to asymmetric strain
Deep embedding leads to symmetric strain
r = 1/ζ
b Multiple shallow insertions in bilayer
Repulsive force
Repulsive force

Fig. 2 | **Hydrophobic insertion (wedging) mechanism of inducing membrane curvature. a** | Single insertion of an amphipathic helix into a monolayer of lipids will locally deform the lipid packing, resulting in a local strain. For clarity, the underlying insertion-free monolayer is not shown. Left: A shallow insertion in a flat monolayer generates an asymmetric strain in packing of lipid acyl chains, and partial relaxation of this strain drives the generation of local curvature in the monoloayer. A particle consisting of the insertion and adjacent lipid molecules has an inverted-cone-like shape, which can be characterized by an intrinsic curvature, ζ, or curvature radius, $r = 1/\zeta$. Right: A deep insertion generates a symmetric strain, which does not result in curvature. Of note, a positive curvature induced in one monolayer causes a positive curvature of the whole bilayer, because the two monolayers are coupled by the hydrophobic interaction (not shown). **b** | Curvature generation by multiple shallow insertions of amphipathic helices occurring in close proximity results in large-scale membrane deformation. The insertions cause deformation of the lipid monolayers they are embedded in, which mediates the interinsertion repulsive forces. The second monolayer, which does not contain insertions, is bent due to the inter-monolayer coupling by hydrophobic interactions.

ENTH domains and Sar1p[41], full-length epsin 1, and carboxy-terminal (C-terminal) domains of epsin 1 and AP180 (REF.[84]). The membrane-anchoring domains of these proteins were replaced with membrane-binding histidine tags, which excluded possible hydrophobic insertions mechanism, but guaranteed protein mobility in the membrane plane by lateral diffusion. Here, the driving force of curvature generation originates from the entropy of the protein distribution across the membrane surface and the related tendency to increase the area available for protein diffusion[41]. This results in a lateral pressure applied within an effective plane, which is parallel to the lipid bilayer surface but elevated above it by a distance roughly equal to the size of the proteins. This slight elevation produces a mechanical lever over which the pressure imposes a torque on the bilayer to generate curvature. The torque and, hence, the curvature strongly and non-linearly increase with the fraction of the membrane area occupied by the protein molecules[41].

The generic nature of the distribution entropy mechanism is attractive. However, a necessary condition for this mechanism is the ability of proteins to undergo unrestricted lateral diffusion in the membrane along with a dense surface concentration. This condition is hardly realizable in intracellular processes. Indeed, in such reactions as the formation of coated vesicles, most proteins are strongly concentrated in a small area, but this is achieved through proteins binding to the clathrin scaffold, which suppresses diffusion and, hence, must by necessity suppress the distribution entropy mechanism.

The internal entropy mechanisms underlie membrane bending by polymeric molecules grafted on membrane surfaces[85–94]. A prominent example of polymers generating membrane curvature in cells is the extracellular plasma membrane glycocalyx[93,95]. Curved surfaces of cilia[96] and filopodia[97] are frequently covered by a high-density glycocalyx consisting of sugar copolymers called 'mucins'[98]. The glycocalyx of hyaluronan and sialic acid polymers covers the strongly curved membranes of neuronal axons[99]. In addition, it has been suggested that disordered domains of multiple membrane-associated proteins exhibit polymer-like physical properties[84,100,101], which implies that they could generate membrane curvature by the same mechanisms as the membrane-associated glycocalyx proteins.

The membrane bending force produced by grafted polymers originates from an intrinsic propensity of a polymer to increase its entropy[102–104]. This principle can manifest itself on the level of an isolated polymer whose end is attached to the membrane (BOX 2) and as a concerted effect of multiple grafted polymers[104]. The latter mechanism comes into play if the membrane coverage by the polymers is so dense that the distance between the grafting points is smaller than the effective dimension of a free polymer coil called the 'polymer gyration radius', R_G, which is referred to as the 'brush' regime (see[105], for example) (FIG. 3a). At such high polymer density, the collisions between the adjacent polymer chains stretch the chains perpendicularly to the membrane surface, which results in a decrease of the chain entropy and a related increase of the chain free energy[104]. Bulging of the grafting membrane in the direction of the polymers provides more space for the polymer chains, which partially relaxes the chain stretching and, hence, reduces the entropy cost[89,91,104]. The accumulation of the entropic free energy of the chains resulting from their stretching can be interpreted as a repulsive interaction between the chains applied in an effective plane parallel to but elevated above the lipid bilayer[87,90,105] (FIG. 3a).

AP180
A protein that plays an important role in clathrin-mediated endocytosis of synaptic vesicles. It is capable of simultaneously binding both membrane lipids (via an ANTH domain) and clathrin, and is therefore thought to recruit clathrin to the membrane of newly invaginating vesicles.

Glycocalyx
A dense, gel-like meshwork of glycoproteins and glycolipids that surrounds the cell, constituting a physical barrier for any object to enter the cell.

This interaction generates a torque, which produces a positive membrane curvature along the whole area covered by the polymer brush[86,91] (FIG. 3a). Estimations show (BOX 2) that the internal entropy mechanism exerted by such grafted polymers as mucins may develop sufficient bending stress to generate large curvatures of radii of $R_S \approx 30$ nm.

It is important to emphasize that, in contrast to the distribution entropy mechanism[41,84], the internal entropy mechanism of polymer brushes does not require the protein anchors to be able to move in the membrane by lateral diffusion, and occurs if the proteins are concentrated by binding of their ends to coats or other protein scaffolds. Therefore, this mechanism is a viable candidate for driving not only the curvature generation by the glycocalyx[93] but also the formation of endocytic buds by the intrinsically disordered domains of the endocytic adaptor proteins epsin 1 and AP180 (REF.[84]).

Box 2 | **Entropic mechanism of curvature generation by grafted polymers**

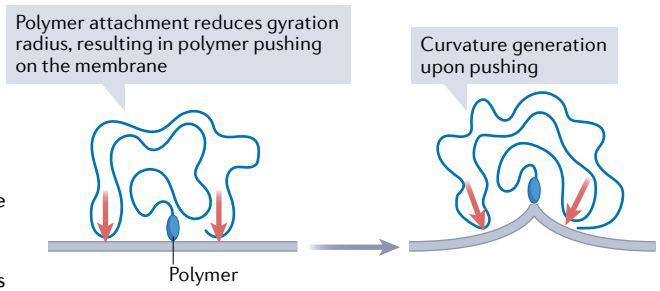
Polymer attachment reduces gyration radius, resulting in polymer pushing on the membrane
Curvature generation upon pushing
Polymer

Curvature generation by isolated polymers may be relevant if the polymer grafting is so sparse that the distance between the grafting points exceeds the polymer gyration radius, R_G. This situation is referred to as the 'mushroom regime' (see[105], for example). Attaching the end of an isolated polymer chain to an initially flat membrane surface reduces by half the space the chain can explore in the course of its conformational excursions, which decreases the overall chain entropy. In a vain attempt to gain back the available space, the chain pushes downwards and bends the membrane region around the attachment point (see the figure)[85,86,89,231,232]. The curvature, J_S, is developed within a membrane spot whose size is set by the gyration radius of the polymer, R_G. The J_S value results from a balance between the effective pressure applied by the chain to the membrane and the membrane resistance to bending quantified by the bending modulus, κ (REF.[223]), and can be estimated according to $J_S = \frac{1}{\sqrt{6\pi}} \frac{k_B T}{4\kappa} \frac{1}{R_G}$ (REF.[232]). If one takes $\kappa \approx 20 k_B T$ (REF.[230]), the estimation of the curvature radius, $R_S = \frac{1}{J_S}$, for mucin polymers characterized by $R_G \approx 32$ nm (REF.[93]) gives $R_S \approx 10^4$ nm, which is two orders of magnitude larger than the typical curvature radii of 10–100 nm characterizing intracellular organelles and transport vesicles. Therefore, internal entropy-based curvature generation by single molecules, although possible, does not appear to be of significant efficiency in cells according to these assumptions.

Curvature generation by densely grafted polymers (FIG. 3a) in the 'polymer brush regime' strongly depends on the distance between the grafting points, ρ. For the case of relatively weak membrane bending, the curvature J_S increases with decreasing ρ according to

$$J_S \approx \frac{5}{24} \frac{k_B T}{\kappa} \frac{R_G^{\frac{10}{3}}}{\rho^{\frac{13}{3}}}$$

(REF.[86]). The area per adaptor protein within clathrin-coated pits is about 60–90 nm^2 (REFS.[84,233]), so the distance between the anchoring points, ρ, can be estimated as about 8–10 nm. Similar and even larger grafting densities corresponding to about 20 nm^2 per polymer attachment point were achieved for mucin in glycocalyx[93]. According to the above equation, the generation of a relevant curvature radius R_S of about 30 nm, for a distance between the grafting points of about 10 nm, requires the polymeric (disordered) protein domains to have gyration radii, R_G, of about 25 nm, which is a biologically feasible value similar to that determined for the glycocalyx polymer mucin[93].

Generic interaction mechanisms

Besides the effective entropic interactions, hydrophilic protein domains in general, and the intrinsically disordered and polymeric domains in particular, often interact through their electric charges[88,93] (FIG. 3b) or due to multiple weak non-covalent bonds referred to as 'multivalent interactions'[106,107] (FIG. 3c). As for entropic interactions, the effective planes of action of both electrostatic and multivalent interactions are parallel to but elevated above the lipid surface (FIG. 3b,c), which results in the development of torques and, hence, the curvature.

Electrostatic interactions are typical for the glycocalyx polymers. These repulsive forces originate from the negative charges of the dissociated acidic groups, which for mucins were estimated to constitute approximately five electron charges per 20 amino acids[93]. The membrane curvature generated by this interaction corresponds to membrane bulging in the direction of the charged polymer and, as such, it is positive (FIG. 3b). A quantitative evaluation of this contribution was done only for erythrocytes and predicted rather small curvature values corresponding to radii on the micrometre scale[95]. Whether the electrostatic interactions have a substantial impact on the curvature of membranes of other cell types remains to be tested both experimentally and theoretically with computational tools[93,95].

The multivalent interactions are attractive[106] and work, therefore, to bring the polymeric or disordered protein domains closer together (FIG. 3c) driving the formation of protein condensates[107]. Such protein interactions can generate membrane bulging away from the surface covered by the proteins so that the resulting membrane curvature is negative. This mechanism is possible only if the membrane anchors of the protein domains are prevented by some factors from approaching each other in the course of condensation (for example, if they were spatially organized by a geometric lattice that held the transmembrane domains apart). While this mechanism of curvature generation has not yet been analysed by modelling, a demonstration of its feasibility has been provided in experiments with the amino-terminal (N-terminal) low-complexity domain of fused in sarcoma (FUS) attached to the surfaces of synthetic and cell-derived membrane vesicles[108].

Scaffolding mechanism

The scaffolding mechanism of membrane curvature occurs when the lipid bilayer moulds into a bent shape through direct attachment of hydrophilic macromolecular complexes that have curvature themselves. This mechanism underlies curvature created by a large variety of proteins, including the relatively small dimers of BAR-domain proteins (for a recent review, see[109]), dimers of sorting nexins (SNXs)[110], core subunits of retromers[111], homopentameric B subunits of Shiga toxins (STxB)[112] and large protein complexes forming spherical cages, which include COPI (REF.[113]) and COPII (REF.[114]) proteins of the secretory vesicles as well as clathrin[115] (see the next section), helical scaffolds of dynamin[116], ESCRT protein complexes[117,118] and lattices of intraviral proteins such as Gag in HIV[119]. Clearly, this is a universally employed mechanism.

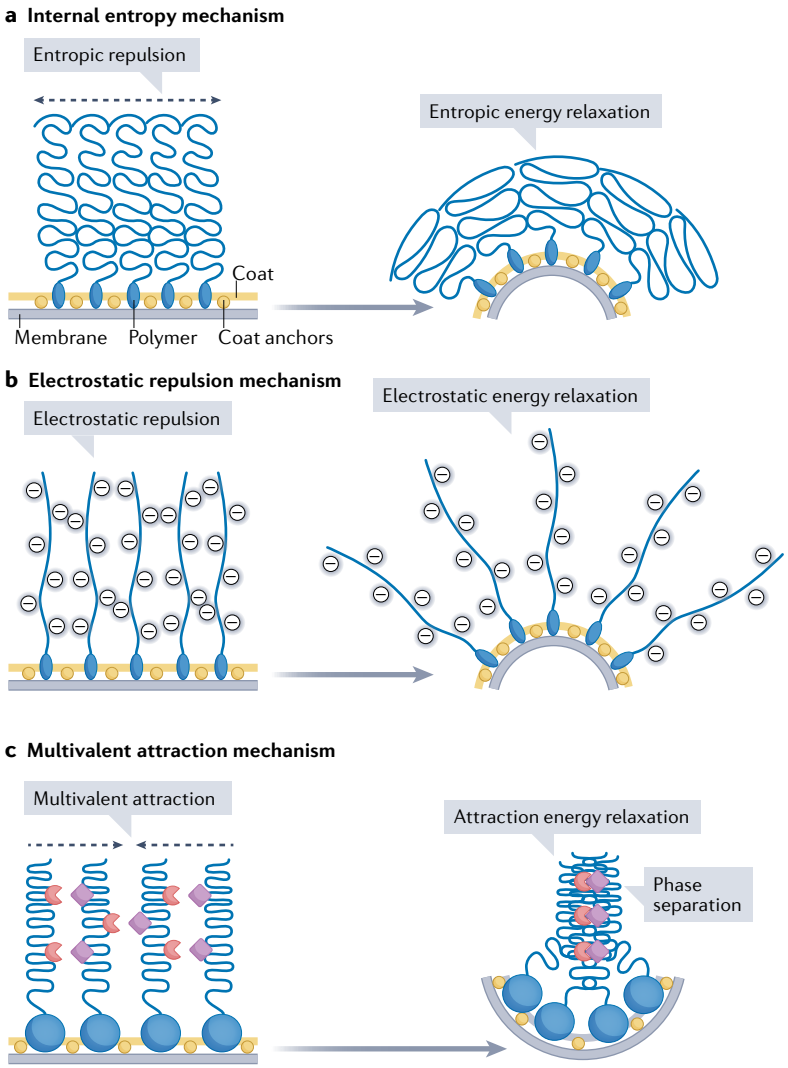

Fig. 3 | **Crowding mechanisms of inducing membrane curvature. a** | Curvature generation by the internal entropy effects of densely grafted polymers (brush regime). Collisions between the adjacent polymer chains stretch the chains perpendicularly to the membrane surface, which results in a decrease of the chain entropy and a related increase of the chain free energy. Bulging of the grafting membrane in the direction of the polymers provides more space for the polymer chains, which partially relaxes the chain stretching and, hence, reduces the entropy cost. **b** | Curvature generation by electrostatic repulsion between densely grafted charged protein domains. The development of a positive membrane curvature allows splaying of the charged domains, which leads to an increase of distance between the charges of adjacent proteins and a resulting decrease of the electrostatic energy. **c** | Curvature generation through multivalent attraction between the hydrophilic protein domains. The attractive interaction tends to decrease the distances between the protein domains, which results in a negative membrane curvature. The dashed arrows indicate the interactions between the proteins driving curvature.

Protein condensates
A class of membraneless organelles and organelle subdomains which carry out specialized functions within the cell and which can form through interaction of protein disordered domains.

For membrane curvature to be generated with a scaffolding mechanism, the effective interface between the curved protein complex and the lipid bilayer must fulfil several requirements. First, the protein scaffold has to be attached to the membrane surface by attractive interactions, which must be stronger than the bilayer resistance to bending. Furthermore, the scaffold has to possess an intrinsically curved shape. And, it has to be more rigid than the lipid bilayer itself. In these conditions, the protein–lipid bilayer interaction originates either from direct attractive forces acting between the proteins and the lipid's polar heads (electrostatic attraction between oppositely charged groups, hydrophobic forces and hydrogen bonding) or from binding to adaptor proteins anchored in the membrane. These two types of interactions are often complementary. In particular, the electrostatic attraction between positively charged protein residues and negatively charged head groups of acidic phospholipids is ubiquitous among scaffolding complexes. These attractive forces between positively charged amino acids (lysine or arginine) and negatively charged lipids are involved in membrane binding by BAR domains[33,120,121], by SNX1 dimers[110], and by SEC23–SEC24–SAR1 heterotrimers mediating COPII-bilayer binding (see the next section). The hydrophobic and hydrogen-bonding forces are involved in STxB pentamer interactions with the glycosphingolipid globotriaosylceramide[122]. The combination of the direct forces must be responsible for binding to a specific lipid, phosphatidylinositol 4,5-bisphosphate, of the pleckstrin-homology domains of dynamin[123] and of AP2 adaptor proteins of clathrin[124]. Anchoring of protein scaffolds within the bilayer is often mediated by small GTPases, which bind membranes through their amphipathic domains. Examples here include SAR1 for COPII and ARF1 for COPI (REF.[20]). While no quantitative evaluations of the strengths of these interactions are available, all the interactions must be strong enough to withstand the resistance of bilayer bending characterized by a bending modulus of about $20k_BT$.

Because these protein–lipid interactions are mediated by specific binding sites, a scaffold is attached to the membrane along several small discrete spots rather than a continuous extended surface. However, the scaffold–bilayer attachment interface is often approximated as a continuous surface, which integrates all the binding sites. Such interfaces for endophilin and amphiphysin were determined on the basis of the positions of the positively charged residues[57]. For Shiga toxin, whose shape appears to be flat, a curved effective attachment interface was built on the basis of an all-atom molecular dynamics simulation of deformations by the protein of globotriaosylceramide-containing lipid bilayers[125,126]. This structural mapping of an attachment interface is one way to evaluate the curvature of a protein scaffold[57,127]. However, the bending rigidity of the attachment interface — which must be larger than that of the lipid bilayer for the curvature generation to be efficient — has never been experimentally evaluated or theoretically confirmed. This interface rigidity must be set by the complex interplay of different factors, including the stiffness of the protein complex, the local flexibilities of the protein regions mediating the membrane attachment and the local flexibilities of the polar lipid heads involved in the interaction.

Membrane curving via protein coats

In cells, the distinct drivers of membrane curvature are coordinated and combined at the nanoscale into highly organized assemblies. In many classical systems, these patches are arranged as a layered coat of dozens of components that act as a platform for bilayer bending, cargo packaging, and signalling[128]. Four of the most well

Sorting nexins
(SNXs). A large group of proteins that are localized in the cytoplasm and have the potential for membrane association either through their lipid-binding PX domain (a phospholipid-binding motif) or through protein–protein interactions with membrane-associated protein complexes.

Retromers
Heteropentameric complexes, which in humans are composed of a less defined membrane-associated sorting nexin (SNX) dimer (SNX1, SNX2, SNX5 and SNX6) and a vacuolar protein sorting (VPS) trimer containing VPS26, VPS29 and VPS35.

Shiga toxins
A family of related toxins with two major groups, Stx1 and Stx2, expressed by genes considered to be part of the genome of lambdoid prophages.

Dynamin
A GTPase responsible for endocytosis in the eukaryotic cell.

ESCRT
The endosomal sorting complexes required for transport (ESCRT) machinery consisting of cytosolic protein complexes, known as ESCRT-0, ESCRT-I, ESCRT-II and ESCRT-III. Together with a number of accessory proteins, these ESCRT complexes enable membrane remodelling that results in membranes bending/budding away from the cytoplasm.

AP2
A multimeric protein that works on the cell membrane to internalize cargo in clathrin-mediated endocytosis.

FCHO2
F-BAR domain-only protein 2, a protein that functions in an early step of clathrin-mediated endocytosis.

ESP15
Epidermal growth factor (EGF) receptor substrate 15, a protein present at clathrin-coated pits in receptor-mediated endocytosis of EGF.

studied systems that organize curvature mechanisms are found in the membrane trafficking system, and include clathrin-coated endocytic pits, COPI and COPII vesicles, and caveolae. Developments in cellular imaging methods over the last two decades (Supplementary Box 1) have allowed the direct mapping of proteins that drive membrane curvature at the nanoscale, even in living cells. These nanoscale, 3D, multicolour and correlative measurements have greatly expanded our understanding of how proteins organize themselves to generate curvature in cells.

Clathrin-based coats

Clathrin-based protein coats provide the primary mechanism of membrane and protein retrieval in eukaryotes[129]. At the heart of clathrin-mediated endocytosis is the formation on the inner surface of the plasma membrane of a bent lattice of clathrin triskelia, the complexes composed of three clathrin heavy chains and three light chains[130]. The membrane attached to the lattice contains and captures cargo and has curvature radii of about 50 nm (REF.[131]). These sites were described over 50 years ago and termed 'bristle-coat membranes'[132,133]. The efficiency and robustness of endocytosis require rigorous control of membrane shaping and cargo capture, which is achieved by a sophisticated and dynamic cast of proteins that likely uses and combines many of the different elementary mechanisms of curvature discussed earlier herein. This complex is built in a stereotyped temporal sequence at the endocytic site[134]. The timing of this process is relatively quick, with single clathrin coats forming and moving into the cell over a period of tens of seconds[135–137]. In the following subsections, we discuss how clathrin coats are formed in time and space, relying on complex combinations of the basic physical mechanisms presented earlier, to drive this key biological mechanism in human cells.

Composition and structure of the clathrin-based coat. Imaging work has shown that as clathrin coats expand and mature on the membrane, modules of proteins including dozens of additional factors load onto the site to shape the membrane, gather cargo and generate forces needed to move the vesicle away from the plasma membrane[129]. In both mammalian cells and yeast, this ordered assembly is stereotypic — leading to membrane fission and vesicle formation[134,138,139]. The nuances of this assembly are distinct in different tissues, and the specific organization and occupancy of the macromolecular structure formed during this process are still unresolved[140]. However, a picture is clearly emerging of how the different layers of the coat and membrane (lipids, cargo, adaptors and clathrin) generally come together to induce curvature[131,141]. Common to these models is the fact that the fundamental organizing framework in the system is the assembly of the outer layer of the clathrin coat itself (FIG. 4a). Specifically, the clathrin lattice forms as a regular array of pentagons and hexagons that assemble into a nanoscale patch of proteins with a defined spacing and geometry[142]. These sites are around 94–133 nm in radius when the clathrin lattice grows as a flat array that can precede curvature across many cell types[143]. This structural lattice is held down to the membrane through the intervening layer of adaptors. The adaptors come in several flavours, with AP2 as the most common in clathrin-mediated endocytosis. The adaptors themselves interact with cargo proteins embedded in the membrane and the membrane itself[144]. Whether the basic lipid composition in these sites is unique is still unresolved, but recent work has highlighted the fact that dynamic signalling lipids, including phosphoinositides, are needed as the coat is recruited and reshaped and the resulting vesicle is cut away from the membrane[145].

Along with the basic layers of the coat, many regulatory and accessory factors are sequentially assembled at these sites (FIG. 4a). These include the epsins, specialized adaptors such as the SNARE adaptor CALM or AP180, several BAR domain-containing proteins, ubiquitin-binding proteins and proteins that modulate and interact with the actin cytoskeleton[129]. The individual roles of many of these proteins inside cells are currently unclear. Specific functions have been proposed biochemically, in vitro and in cells. But how the factors assemble together, and what functional role they play together as a collective, is yet to be fully understood. Indeed, many of the individual factors exhibit dual or overlapping roles, making it difficult for simple mutagenesis or knockdown to disentangle their roles completely or in isolation. For example, a complete perturbation of dynamin in cells required removal of all three isoforms (dynamin 1, dynamin 2 and dynamin 3)[146]. The essential nature of endocytosis has made the system in many ways resistant to severe perturbation and classic single-protein mechanistic dissection.

Temporal sequence of the component recruitment. Classically, the clathrin coat is thought to form first by the stochastic capture of adaptor proteins and clathrin by membrane-associated cargo proteins[147]. Specifically, AP2 adaptor proteins and clathrin triskelia are recruited to the membrane. These initial complexes are stabilized by crosslinking early-arriving accessory factors, including FCHO2, ESP15 and intersectin[148,149]. The coat then grows at the membrane, captures additional cargo and is reshaped into a vesicle. Other work has suggested that earlier events may precede this nucleation. Specifically, the assembly of some factors, including FCHO2, EPS15 and intersectin, by interactions with phosphoinositides might occur shortly before the assembly of the adaptor layer[150]. These nascent nucleation sites and, possibly, natural, nanometre-scale undulations of the membrane itself would be the trigger to form an endocytic site. This nanoscale site is further assembled either through multivalency binding interactions forming clusters or through a liquid–liquid phase transition among domains of these early-arriving molecules resulting in the formation of a condensate[151,152].

Spatial distribution of the components. Recent super-resolution and correlative light and electron microscopy of the proteins that assemble together with the clathrin coat has been illuminating to determine the distributions

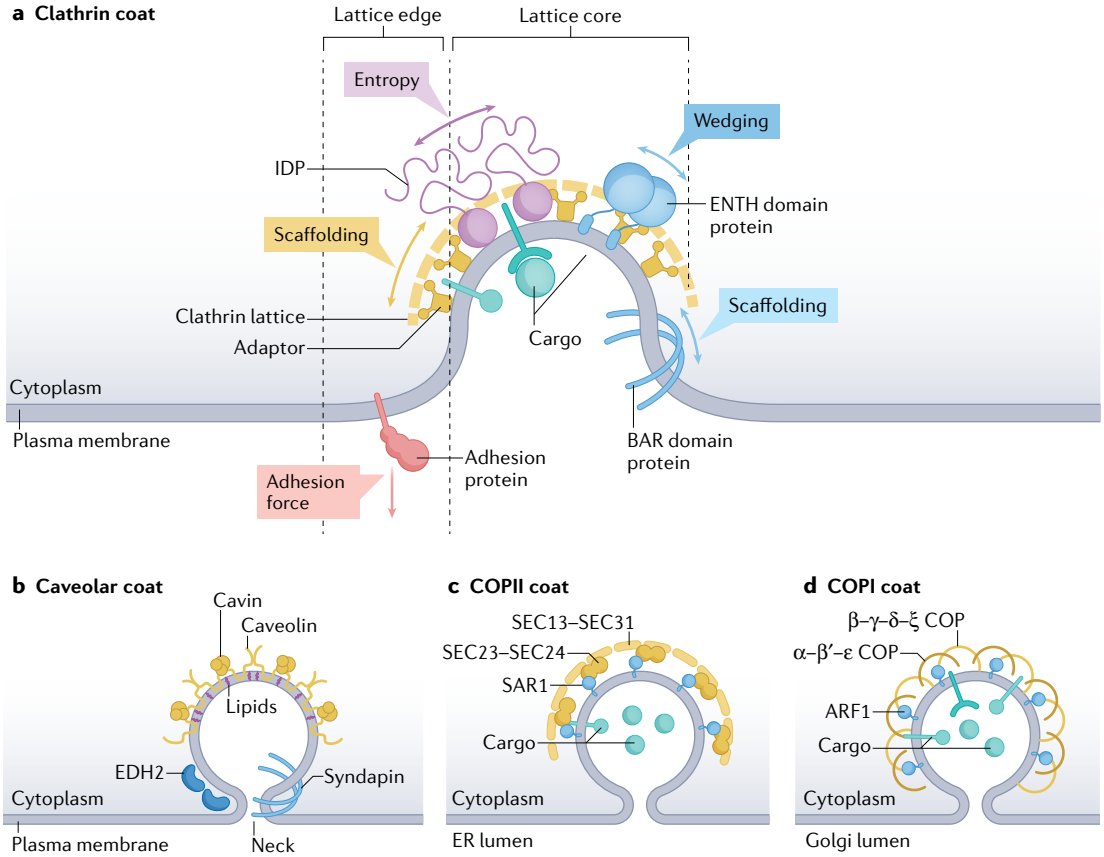

Fig. 4 | **Curvature generation by protein coats. a** | Cartoon of the local organization of the key proteins involved in bending the clathrin coat at the plasma membrane. Different factors, including BAR domain proteins, cargo, intrinsically disordered proteins (IDPs), adaptors, and the clathrin lattice, assemble in a specific pattern in relation to the edge of the lattice formed by clathrin triskelia. Forces generated by distinct mechanisms on the membrane induced by these individual factors are likely to produce a complex energy landscape depending on how concentrated and active each factor is in bending the membrane and where specifically each factor is located at the nanoscale. The combination of these multiple and diverse factors and forces helps shape the clathrin-coated pit into a sphere. Specifically, the clathrin lattice produces a scaffolding force as it bends to a preferred spherical curvature. IDP domains can induce positive curvature forces through entropy. BAR domain proteins can scaffold curvature. Adhesion forces through integrins interacting with the extracellular matrix can produce a holding force that keeps the lattice flat. How these individual factors and their forces are organized and activated at the nanoscale results in the complex pathways of curvature. **b** | Cartoon of the local organization of the key proteins involved in forming caveolae at the plasma membrane. Different factors, including the ATPase EHD2, CAVINs, caveolin and the BAR domain protein syndapin, assemble to form these small clustered domains that concentrate specific lipids. **c** | Cartoon of the local organization of the key proteins involved in the COPII-coated domain. Different factors, including SAR1, SEC23–SEC24 and the coat SEC13–SEC31, assemble in a layered fashion similar, in principle, to the layered clathrin coat to organize cargo. **d** | In the COPI coat, the proteins ARF1, α–β′–ε COP and β–γ–δ–ζ COP assemble in a more interwoven structure to generate a curved organelle that concentrates cargo. ER, endoplasmic reticulum.

Intersectin
A cytoplasmic membrane-associated protein that indirectly coordinates endocytic membrane trafficking with the actin assembly machinery.

β-Arrestins
Multifunctional intracellular proteins with an ability to directly interact with a large number of cellular partners.

DAB2
Disabled 2, a clathrin- and cargo-binding endocytic adaptor protein recognized for its multifaceted roles in signalling pathways.

HIP1R
A component of clathrin-coated pits and vesicles that may link the endocytic machinery to the actin cytoskeleton.

and positions of the proteins that assemble together with the clathrin lattice at the nanoscale[153]. The proteins that assemble with clathrin have been shown to assemble into four general zones in relation to the edge of the lattice. First, the most central zone contains some cargo and ligand-specific adaptors. These include the epsins, CALM, SNAREs and the cargo. The edge of the lattice is strongly populated by several important endocytic proteins, including ESP15, FCHO1/2 and dynamin. A set of proteins, including amphiphysin and syndapin (also known as PACSIN), assembles more distally to the edge. Finally, a group of proteins appears to transition between the edge and the central zone. These include β-arrestins, AP2, DAB2 and some actin-binding proteins, including HIP1R and intersectin. Together, there is a dynamic movement between these general zones during curvature generation[154].

While the nanoscale locations of these factors are known, how they directly bind to one another and dynamically assemble and gather cargo has not yet been determined. Dynamic phosphorylation events, conformational switching, ubiquitylation, allostery and, likely, domain-specific rearrangements allow factors to engage and disengage across the structure. As many of the factors have PRD and SH3 domains or other common binding motifs that can be readily exchanged, these factors can engage in local stepwise and coordinated assembly[155,156].

Curvature generation. Considering the known proteins that associate with clathrin-based coats, a set of factors are present during endocytosis that have the potential to use all of the elementary mechanisms of curvature generation. This includes epsins, endophilin, amphiphysin and CALM, whose amphipathic helices can generate curvature by the hydrophobic insertion mechanism. The intrinsically disordered full-length epsin 1 and the C-terminal domains of epsin 1 and AP180 can produce curvature by the internal entropy mechanism. The BAR domains of endophilin, amphiphysin and FCHO1/2, as well as clathrin lattice itself, and dynamin oligomers can create curvature through scaffolding. One major player that has emerged as a regulator of curvature generation by an unknown mechanism is the AP2 adaptor complex or similar adaptors[157,158].

Concerted or sequential actions of all these factors provide the coat with a robust ability to generate membrane curvature. Indeed, when the top of a cell adhered to a substrate is removed and the remaining exposed membrane is washed of ATP/GTP and soluble factors, the clathrin coat has been shown to spontaneously curve from flat and domed shapes into fully spherical vesicles[143,159]. Here, the energy for curvature is intrinsically contained in the clathrin lattice itself, the membrane and the protein factors associated with it[143,160,161]. Clearly, no additional factors, added energy or cytoskeletal polymerization is inherently required to curve the clathrin coat in plasma membranes of eukaryotic cells[162].

Challenges in understanding membrane bending by clathrin coats. How do the multiple curvature-generating proteins work together to specifically shape the membrane of a clathrin site into a spherical vesicle? Past work centred on the relationship between the physical nature of coat assembly and curvature generation. Two competing nanoscale models have been proposed[131,163]. In one scenario, called the 'rising sun model', the coat assembles with a set curvature and grows into a sphere. In the other extreme model, called the 'constant area model', the coat assembles to a final flat area, and then curves into a sphere by reducing its overall radius without additional clathrin added to the coat. Recent work has shown that mixtures of the two actually occur in living cells[164,165]. Some clathrin-coated sites grow with constant curvature, others grow flat and then curve midway before scission, and some grow flat to a final size and then curve[143,165]. These different pathways can exist even within the same cell and in the same small patch of the plasma membrane. The specific regulators of this behaviour are unclear and must be acting with nanoscale precision. Furthermore, how specific protein species located on and around the coat control the transition from flat to curved is also unclear. What is clear, however, is that the clathrin lattice is quite flexible and can accommodate many different pathways of curvature[143]. How this is modulated and controlled in different cells and what the specific scenarios are is a rich area for current and future investigation[134,158,160]. However, past work suggesting that clathrin lattices require extensive geometrical reordering was shown to be incorrect. Most flat lattices in cells contain many pentagons that would be required to curve into a sphere, abrogating the need to reorder a purely hexagonal flat lattice upon curving[143].

If curvature is preferred, why does the clathrin-based coat sometimes grow flat[166]? Likewise, what drives the curvature transition of the flat coat? The lowest-energy state of the bare clathrin lattice is the spherical basket. When free triskelia are allowed to assemble in solution, they assume the spherical cage geometry with and without membrane and adaptors[167]. Thus, growth of the clathrin-based coat in the flat state is not energetically favourable, and the presence of flat coats in living cells implies there are forces holding the coat flat, and inhibiting its curving[143,160]. Work has shown that in the flat state the clathrin lattice is disordered, and the coat is held flat likely by adhesion proteins such as integrins[143,168]. When this force is removed, the coats curve.

How does the clathrin coat curve? In one scenario, the clathrin lattice can be thought of as a locked ratchet waiting for an adhesive holding force to be released so that the lattice can relax back to its natural low-energy curved 'basket' state[131]. Bound proteins would aid in this process by shaping or scaffolding the curvature pathway. Here, the accessory proteins can be thought of as regulators rather than actively recruited energy-dependent drivers of the natural process of curving the coat into a vesicle[162]. Thus, the clathrin lattice itself would provide the force necessary for curvature with the help of these accessory factors. This model would be consistent with both the 'rising sun' scenario and the 'constant area' scenario of endocytosis discussed above.

Another current challenge in understanding clathrin-mediated endocytosis is evaluating how the specific curvature and shaping mechanisms are organized in and around a coat at the nanoscale. From super-resolution imaging, we can position many of the proteins within single clathrin coats in mammalian cells. Similar data have been generated in yeast[169]. Surprisingly, it was found that many protein domains that support curvature (for example, FCHO2 and the disordered domains of epsins and CALM) are organized in different zones around the coat. However, only a few proteins seem to have a concentration that changes during the curvature transition. These were specifically CALM, VAMP2, SNX9 and dynamin. In this regard, the classic curvature-generating proteins such as BAR-domain proteins and intrinsically disordered proteins, including epsin, were found even in flat clathrin lattices. Thus, conformational changes, post-translational changes (that is, phosphorylation) or other activities must be controlling whether and when these proteins use their specific curvature-generating actions on the membrane during vesicle shaping.

Caveolin-based coats

Caveolae are spherical bulb-like pits with a diameter of about 90 nm which form on the cytoplasmic face of the plasma membrane and are common in certain cell types, such as epithelial cells, fat cells, glia and muscle cells[170,171]. Functionally, caveolae have been implicated in mechanical protection of cells[29,156,172]. It has been

suggested that when a cell is subjected to an extreme stretch, caveolae flatten, acting as membrane reservoirs to protect the plasma membrane from rupture[173,174]. Another recognized function of caveolae is the internalization of lipids, which are proposed to be one of the primary cargos of caveolae[156]. Thus, caveolae and the vesicles formed upon their separation from the plasma membrane move lipids throughout the cell and into lipid droplets. Protein cargo-based triggering of the assembly of adaptors and coats is not thought to generally occur in this system. However, different lipids have been shown to affect the residence time, diffusion and shape of caveolae[175]. In this regard, the underlying nature of the membrane itself likely has a central role in the curvature and scission pathway of caveolae. The distinctive and homogeneous size of caveolae suggests that the curvature of caveolae is highly regulated by a set of specific elementary mechanisms[176].

Composition and structure. How do caveolae curve? Unlike clathrin structures, caveolin-based coats are formed from a relatively limited set of core proteins[21,176] (FIG. 4b). These include the integral membrane proteins caveolin 1, caveolin 2 and caveolin 3, which form shallow discs inserted into the membrane, the cytosolic coat proteins CAVIN1, CAVIN2 and CAVIN3, the ATPase EHD2, EH domain-binding protein 1 (EHBP1) and the actin-binding BAR domain-containing protein syndapin. Additional signalling proteins have been assigned to the caveolin domain (for example, proteins involved in endothelial nitric oxide synthase signalling[177]). In some specialized cells, such as endothelial cells, the protein PV1 is thought to assemble a unique wagon wheel-like structure at the neck of caveolae[178]. Altogether, this limited set of components assembles into small unitary invaginations that gather and cluster lipids, including cholesterol and sphingomyelin.

The membrane protein caveolin is the fundamental building block of caveolae, having its N and C termini in the cytosol and intramembrane domains embedded in the bilayer[179]. Mutants, overexpression and downregulation of caveolin have been associated with diseases across many systems, including cancer, cardiovascular disease, and muscle function[180]. The recruited cytosolic CAVIN coat proteins are the most abundant factors that assemble with caveolins, creating a basic two-layered coat. Distinctive spirals and stripes of CAVINs have been observed assembling on flat and curved caveolae for decades with platinum replica and transmission electron microscopy[179]. The timing for the assembly of these structures is much slower than clathrin-mediated endocytosis. A stepwise assembly of the coat occurs over several minutes at the plasma membrane[176,181]. However, caveolae can be quite dynamic in the cytosol as rapidly transported organelles.

Curvature generation. The layered caveolin–CAVIN complex is proposed to drive membrane curvature by combining the elementary curvature mechanisms provided by the core components of caveolin, CAVINs, syndapin and EHD2 (REF.[21]). For example, when expressed in bacteria, caveolin itself can form small vesicles that can bud from the bacterial membrane[182]. Here, the presence of caveolin is sufficient to generate both membrane curvature and scission of a vesicle. It is possible that the rather simple composition and organization of the bacterial membrane allows the caveolin alone to form vesicles by an unknown mechanism, whereas in more complex eukaryotic cells, with their specific membrane tensions, glycocalyx and cytoskeleton, additional factors, such as CAVINs[183,184], are needed.

Recent work has suggested that CAVINs contain intrinsically disordered domains that can induce curvature by the internal entropy mechanism[185]. In addition, phosphorylation sites in the cytosolic domains of CAVINs can provide electric charges and could induce membrane curvature by the electrostatic mechanism[186]. Likewise, EHD2 and syndapin have BAR domains, and could contribute to curvature by the scaffolding mechanism. Indeed, mutations of syndapin result in mostly flat or disassembled caveolae[187,188].

Similarly to the formation of clathrin-coated pits, the challenge of the flat-to-curved transition exists also for caveolin-based coats, which have been observed in these two general states. What factors regulate the transition between these two shapes of caveolae and their functional role in the cell is still unresolved.

COP-based coats

The two other major coats in eukaryotic cells which form as nanoscale patches on the cytoplasmic face of membranes and bend membranes into enclosed trafficking vesicles are COPI and COPII coats[10,189]. COPI/II-coated vesicles mediate trafficking between the ER and the Golgi apparatus, while COPI vesicles are responsible for the transport within the Golgi apparatus itself.

Composition and structure. For the COPII coat, a membrane-resident ER protein, SEC12, activates nucleotide exchange in SAR1 to trigger the insertion of its N-terminal amphipathic helix into the ER membrane (FIG. 4c). SAR1 then recruits the two additional layers of the COPII coat composed of the SEC23–SEC24 heterodimer to form an inner shell and the SEC13–SEC31 heterodimer to form an outer shell. These structural elements are able to build a flexible lattice-like coat that can recruit cargo of various sizes into the vesicle. These lattices can be assembled in many different geometries[190]. While the underlying structures and interfaces are similar, small kinks, flipping of subunits, occupancy changes within the layers and changes in the angles of the interactions allow more global changes to the overall extended lattice architecture. The inner coat layer of SEC23–SEC24 forms mostly a helical array that can interact with the outer rod layers. This flexible layering of the coat permits the assembly of differently shaped COPII vesicles, including spheres and tubules, that could package even exceptionally large cargos, including collagen fibres. Here, the coat arrangement appears to shape the membrane through its overall extended architecture. The timing of COPII dynamics is also thought to be relatively slow compared with that of clathrin-coated structures. COPII sites are fairly slow to turnover and

relatively immobile, which allows the coats to selectively incorporate specific cargo[191,192].

Similarly to COPII coat assembly, COPI coat assembly is mediated by a small GTPase, ARF1, and a heteroheptameric protein coat complex formed by COP proteins (so-called coatomer) (FIG. 4d). Mirroring the COPII pathway, in the COPI pathway, a Golgi apparatus-resident nucleotide exchange factor, GBF1, activates ARF1 to insert an N-terminal myristolyated amphipathic α-helix into the Golgi membrane[193]. This membrane-associated protein then recruits the coat as a fully assembled highly interlaced basket-like unit. A tetrameric complex of β, γ, δ and ζ subunits creates an adapter-like structure, while a trimeric subcomplex of α–β′–ε COP forms a lattice-like cage structure. The basic building block is a triad of membrane-bound ARF1 proteins, which are linked by associations with the COPI subunits, and are interwoven into a single curved layer that can interact with and gather cargo molecules[194]. Unlike in the COPII pathway, the vesicles in this pathway appear to be smaller and more homogeneous in size and cannot accommodate large cargos[113,195].

Curvature generation. The initial event thought to drive membrane curvature in the COPII coat is the insertion of the SAR1 N-terminal amphipathic α-helix into the membrane[196]. This insertion would induce membrane bending according to the hydrophobic insertion mechanism. When this domain is removed or mutated, SAR1 is unable to tubulate membranes. However, recruitment of the inner coat of SEC23–SEC24 and the outer coat of SEC13–SEC31 is also able to induce tubules, which is likely driven by the scaffolding mechanism. Thus, a sequence of membrane destabilizations by SAR1 is enhanced by the assembly of the inner and outer coats of COPII. Specific rearrangements in this layering process shape the vesicle into unique and specific morphologies to accommodate the diverse cargo of the ER and Golgi apparatus. For the COPI coat, a likely contributor to curvature generation is the insertion of the ARF1 N-terminal helix[197,198]. Whether the other COPI-coat components have effects on membrane curvature remains to be revealed. Likewise, whether other components are organized at the nanoscale around COP coats is unknown. Finally, what creates the initial recruitment zone at the ER/Golgi membranes is unclear.

Conclusions

Proteins can produce membrane curvature by many distinct mechanisms, each based on different physical principles. As outlined in this Review, the chief mechanisms generating nanoscale curvatures of intracellular membranes are the hydrophobic insertion mechanism driven by asymmetric embedding of a protein domain into the lipid bilayer; scaffolding mechanisms based on attachment of a curved protein complex to the membrane surface; and versions of crowding mechanisms fuelled by the entropy of polymer-like regions of disordered hydrophilic domains densely grafted onto the membrane surface. These three major classes can, in principle, explain the shaping of all known membrane configurations within eukaryotic cells. However, many questions remain. Specifically, how do the curvature-generating proteins concentrate at sites committed to shaping, which include macroscopically large membrane arrays such as ER and Golgi ribbons and the nanoscopic sites of endocytic vesicles. Within single sites of curvature, the numbers and distributions of these proteins would strongly influence bending and shaping events. There are high energetic barriers to overcome to change a membrane shape, including entropic forces, repulsive forces mediated by membrane deformations and other repulsive forces between the curvature-generating proteins. Likewise, understanding the roles of coats in combination, organization and local coordination in time and space of different curvature generation mechanisms is key. Are coats acting as master regulators of this process or as passive scaffolds? Do coats position proteins at specific locations within the membrane with defined spacings? Lastly, as coats can be organized in different ways — including multiprotein layered structures or more complex interwoven structures — it will be important to understand what roles these different arrangements play in selecting membrane locations where coats assemble with common functional properties such as plasticity and the ability to undergo confined shape transitions. Even further, it is critical to understand how layers of the coat transmit forces between the membrane and protein layers to balance and coordinate shaping interactions. How is this controlled to produce different shapes? Clearly, much work remains to be done to understand the dynamics of the proteins that shape membranes and how cells use them to support their architecture and function.

How might these challenges be addressed? First, the curvature of coats occurs at a scale that pushes the resolution of classic imaging methods. For an atomic view of how these structures assemble and interact, atomic-level structures are needed. These could be generated both in vitro and inside cells with cryogenic electron microscopy and cryogenic electron tomography methods. Structures of assembled components of the coats or fully assembled native cellular organelles could be solved. Because these events are highly dynamic and heterogeneous, new ultra-high-resolution, fast and conformationally sensitive live-cell imaging of multiple components is needed (Supplementary Box 1). Again, achieving single-molecule resolution of imaging to visualize — in live cells or advanced reconstitution systems — single proteins assembling, interacting and conformationally changing is key to understanding how coats drive curvature. Lastly, modelling these interactions to reveal how they work from a first-principles physics and chemistry perspective will be, in the end, key to being able to understand, predict and manipulate these systems that are working in the complex environment of cells and tissues. Using these paths to solve these challenges will result in a detailed mechanistic view of how proteins use elemental physical properties in unison to shape and build organelles within the cell.

Published online 2 August 2022

1. Doherty, G. J. & McMahon, H. T. Mechanisms of endocytosis. *Annu. Rev. Biochem.* **78**, 857–902 (2009).
2. Ishikawa, H. Formation of elaborate networks of T-system tubules in cultured skeletal muscle with special reference to the T-system formation. *J. Cell Biol.* **38**, 51–66 (1968).
3. Yeow, I. et al. EHD proteins cooperate to generate caveolar clusters and to maintain caveolae during repeated mechanical stress. *Curr. Biol.* **27**, 2951–2962.e2955 (2017).
4. Lo, H. P. et al. The caveolin–cavin system plays a conserved and critical role in mechanoprotection of skeletal muscle. *J. Cell Biol.* **210**, 833–849 (2015).
5. Franzini-Armstrong, C. The relationship between form and function throughout the history of excitation–contraction coupling. *J. Gen. Physiol.* **150**, 189–210 (2018).
6. Lo, H. P. et al. Cavin4 interacts with Bin1 to promote T-tubule formation and stability in developing skeletal muscle. *J. Cell Biol.* https://doi.org/10.1083/JCB.201905065/VIDEO-1 (2021).
7. Westrate, L. M., Lee, J. E., Prinz, W. A. & Voeltz, G. K. Form follows function: the importance of endoplasmic reticulum shape. *Annu. Rev. Biochem.* **84**, 791–811 (2015).
8. Guo, Y. et al. Visualizing intracellular organelle and cytoskeletal interactions at nanoscale resolution on millisecond timescales. *Cell* **175**, 1430–1442.e1417 (2018).
9. Nixon-Abell, J. et al. Increased spatiotemporal resolution reveals highly dynamic dense tubular matrices in the peripheral ER. *Science* **354**, aaf3928 (2016).
10. Weigel, A. V. et al. ER-to-Golgi protein delivery through an interwoven, tubular network extending from ER. *Cell* https://doi.org/10.1016/j.cell.2021.03.035 (2021).
11. Ladinsky, M. S., Mastronarde, D. N., McIntosh, J. R., Howell, K. E. & Staehelin, L. A. Golgi structure in three dimensions: functional insights from the normal rat kidney cell. *J. Cell Biol.* **144**, 1135–1149 (1999).
12. Kalt, M. R. Mitochondrial pleiomorphism in sustentacular cells of Xenopus laevis. *Anat. Rec.* **182**, 53–60 (1975).
13. Bornstein, S. R., Ehrhart-Bornstein, M., Guse-Behling, H. & Scherbaum, W. A. Structure and dynamics of adrenal mitochondria following stimulation with corticotropin releasing hormone. *Anat. Rec.* **234**, 255–262 (1992).
14. Bussi, Y. et al. Fundamental helical geometry consolidates the plant photosynthetic membrane. *Proc. Natl Acad. Sci. USA* **116**, 22366–22375 (2019).
15. De Matteis, M. A. & Luini, A. Exiting the Golgi complex. *Nat. Rev. Mol. Cell Biol.* **9**, 273–284 (2008).
16. Zimmerberg, J. & Kozlov, M. M. How proteins produce cellular membrane curvature. *Nat. Rev. Mol. Cell Biol.* **7**, 9–19 (2005).
17. Omar, Y. A. D., Sahu, A., Sauer, R. A. & Mandadapu, K. K. Nonaxisymmetric shapes of biological membranes from locally induced curvature. *Biophys. J.* **119**, 1065–1077 (2020).
18. Vasan, R., Rudraraju, S., Akamatsu, M., Garikipati, K. & Rangamani, P. A mechanical model reveals that non-axisymmetric buckling lowers the energy barrier associated with membrane neck constriction. *Soft Matter* **16**, 784–797 (2020).
19. Auddya, D. et al. Biomembranes undergo complex, non-axisymmetric deformations governed by Kirchhoff-Love kinematics and revealed by a three-dimensional computational framework. *Proc. Math. Phys. Eng. Sci.* **477**, 20210246 (2021).
20. Faini, M., Beck, R., Wieland, F. T. & Briggs, J. A. G. Vesicle coats: structure, function, and general principles of assembly. *Trends Cell Biol.* **23**, 279–288 (2013).
21. Parton, R. G., Tillu, V., McMahon, K. A. & Collins, B. M. Key phases in the formation of caveolae. *Curr. Opin. Cell Biol.* **71**, 7–14 (2021).
22. Margolis, L. & Sadovsky, Y. The biology of extracellular vesicles: the known unknowns. *PLoS Biol.* **17**, e3000363 (2019).
23. Hu, J., Prinz, W. A. & Rapoport, T. A. Weaving the web of ER tubules. *Cell* **147**, 1226–1231 (2011).
24. Mattila, P. K. & Lappalainen, P. Filopodia: molecular architecture and cellular functions. *Nat. Rev. Mol. Cell Biol.* **9**, 446–454 (2008).
25. Cramer, L. P. & Mitchison, T. J. Investigation of the mechanism of retraction of the cell margin and rearward flow of nodules during mitotic cell rounding. *Mol. Biol. Cell* **8**, 109–119 (1997).
26. Terasaki, M. et al. Stacked endoplasmic reticulum sheets are connected by helicoidal membrane motifs. *Cell* **154**, 285–296 (2013).
27. Mizushima, N., Yoshimori, T. & Ohsumi, Y. The role of Atg proteins in autophagosome formation. *Annu. Rev. Cell Dev. Biol.* **27**, 107–132 (2011).
28. Shin, W. et al. Preformed Ω-profile closure and kiss-and-run mediate endocytosis and diverse endocytic modes in neuroendocrine chromaffin cells. *Neuron* **109**, 3119–3134.e3115 (2021).
29. Parton, R. G. Caveolae: structure, function, and relationship to disease. *Annu. Rev. Cell Dev. Biol.* **34**, 111–136 (2018).
30. Golani, G., Ariotti, N., Parton, R. G. & Kozlov, M. M. Membrane curvature and tension control the formation and collapse of caveolar superstructures. *Dev. Cell* **48**, 523–538.e524 (2019).
31. Shemesh, T. et al. A model for the generation and interconversion of ER morphologies. *Proc. Natl Acad. Sci. USA* **111**, E5243–E5251 (2014).
32. Schroeder, L. K. et al. Dynamic nanoscale morphology of the ER surveyed by STED microscopy. *J. Cell Biol.* **218**, 83–96 (2019).
33. Mcmahon, H. T. & Boucrot, E. Membrane curvature at a glance. *J. Cell Sci.* **128**, 1065–1070 (2015).
34. Bhatia, T., Christ, S., Steinkühler, J., Dimova, R. & Lipowsky, R. Simple sugars shape giant vesicles into multispheres with many membrane necks. *Soft Matter* **16**, 1246–1258 (2020).
35. Bo, L. & Waugh, R. E. Determination of bilayer membrane bending stiffness by tether formation from giant, thin-walled vesicles. *Biophys. J.* **55**, 509–517 (1989).
36. Zhao, Z. et al. Super-resolution imaging of highly curved membrane structures in giant vesicles encapsulating molecular condensates. *Adv. Mater.* https://doi.org/10.1002/adma.202106633 (2021).
37. Karimi, M. et al. Asymmetric ionic conditions generate large membrane curvatures. *Nano Lett.* **18**, 7816–7821 (2018).
38. Has, C. & Das, S. L. Recent developments in membrane curvature sensing and induction by proteins. *Biochim. Biophys. Acta Gen. Subj.* **1865**, 129971 (2021).
39. Ford, M. G. et al. Curvature of clathrin-coated pits driven by epsin. *Nature* **419**, 361–366 (2002).
40. Campelo, F., McMahon, H. T. & Kozlov, M. M. The hydrophobic insertion mechanism of membrane curvature generation by proteins. *Biophys. J.* **95**, 2325–2339 (2008).
41. Stachowiak, J. C. et al. Membrane bending by protein-protein crowding. *Nat. Cell Biol.* **14**, 944–949 (2012).
42. Farsad, K. & De Camilli, P. Mechanisms of membrane deformation. *Curr. Opin. Cell Biol.* **15**, 372–381 (2003).
43. Gallop, J. L. & McMahon, H. T. BAR domains and membrane curvature: bringing your curves to the BAR. *Biochem. Soc. Symp.* https://doi.org/10.1042/bss0720223 (2005).
44. Cooke, I. R. & Deserno, M. Coupling between lipid shape and membrane curvature. *Biophys. J.* **91**, 487–495 (2006).
45. Carlsson, A. E. Membrane bending by actin polymerization. *Curr. Opin. Cell Biol.* **50**, 1–7 (2018).
46. Blood, P. D., Swenson, R. D. & Voth, G. A. Factors influencing local membrane curvature induction by N-BAR domains as revealed by molecular dynamics simulations. *Biophys. J.* **95**, 1866–1876 (2008).
47. Li, Z.-L. Molecular dynamics simulations of membrane deformation induced by amphiphilic helices of epsin, Sar1p, and Arf1. *Chin. Phys. B* **27**, 038703 (2018).
48. Sodt, A. J. & Pastor, R. W. Molecular modeling of lipid membrane curvature induction by a peptide: more than simply shape. *Biophys. J.* **106**, 1958–1969 (2014).
49. Zemel, A., Ben-Shaul, A. & May, S. Membrane perturbation induced by interfacially adsorbed peptides. *Biophys. J.* **86**, 3607–3619 (2004).
50. Zemel, A., Ben-Shaul, A. & May, S. Modulation of the spontaneous curvature and bending rigidity of lipid membranes by interfacially adsorbed amphipathic peptides. *J. Phys. Chem. B* **112**, 6988–6996 (2008).
51. Spivak, M. *A Comprehensive Introduction to Differential Geometry* (Brandeis University, 1970).
52. Drin, G. & Antonny, B. Amphipathic helices and membrane curvature. *Febs Lett.* **584**, 1840–1847 (2010).
53. Cornell, R. & Taneva, S. Amphipathic helices as mediators of the membrane interaction of amphitropic proteins, and as modulators of bilayer physical properties. *Curr. Protein Pept. Sci.* **7**, 539–552 (2006).
54. Segrest, J. P., Garber, D. W., Brouillette, C. G., Harvey, S. C. & Anantharamaiah, G. M. The amphipathic alpha helix: a multifunctional structural motif in plasma apolipoproteins. *Adv. Protein Chem.* **45**, 303–369 (1994).
55. Giménez-Andrés, M., Čopič, A. & Antonny, B. The many faces of amphipathic helices. *Biomolecules* **8**, 45 (2018).
56. Ambroso, M. R., Hegde, B. G. & Langen, R. Endophilin A1 induces different membrane shapes using a conformational switch that is regulated by phosphorylation. *Proc. Natl Acad. Sci. USA* **111**, 6982–6987 (2014).
57. Gallop, J. L. et al. Mechanism of endophilin N-BAR domain-mediated membrane curvature. *EMBO J.* **25**, 2898–2910 (2006).
58. Kweon DH, S. Y. et al. Membrane topology of helix 0 of the epsin N-terminal homology domaintle. *Mol. Cell* **21**, 428–435 (2006).
59. Isas, J. M., Ambroso, M. R., Hegde, P. B., Langen, J. & Langen, R. Tubulation by amphiphysin requires concentration-dependent switching from wedging to scaffolding. *Structure* **23**, 873–881 (2015).
60. Varkey, J. et al. Membrane curvature induction and tubulation are common features of synucleins and apolipoproteins. *J. Biol. Chem.* **285**, 32486–32493 (2010).
61. Herrick, D. Z., Sterbling, S., Rasch, K. A., Hinderliter, A. & Cafiso, D. S. Position of synaptotagmin I at the membrane interface: cooperative interactions of tandem C2 domains. *Biochemistry* **45**, 9668–9674 (2006).
62. Rufener, E., Frazier, A. A., Wieser, C. M., Hinderliter, A. & Cafiso, D. S. Membrane-bound orientation and position of the synaptotagmin C2B domain determined by site-directed spin labeling. *Biochemistry* **44**, 18–28 (2005).
63. Wang, N. et al. Mechanism of membrane-curvature generation by ER-tubule shaping proteins. *Nat. Commun.* **12**, 1–15 (2021).
64. Ergüder, M. F. & Deserno, M. Identifying systematic errors in a power spectral analysis of simulated lipid membranes. *J. Chem. Phys.* https://doi.org/10.1063/5.0049448 (2021).
65. Hamm, M. & Kozlov, M. M. Tilt model of inverted amphiphilic mesophases. *Eur. Phys. J. B Condens. Matter Complex. Syst.* **6**, 519–528 (1998).
66. Hamm, M. & Kozlov, M. M. Elastic energy of tilt and bending of fluid membranes. *Eur. Phys. J. E* **3**, 323–335 (2000).
67. Terzi, M. M., Ergüder, M. F. & Deserno, M. A consistent quadratic curvature-tilt theory for fluid lipid membranes. *J. Chem. Phys.* **151**, 164108 (2019).
68. Campelo, F., Fabrikant, G., McMahon, H. T. & Kozlov, M. M. Modeling membrane shaping by proteins: focus on EHD2 and N-BAR domains. *FEBS Lett.* **584**, 1830–1839 (2010).
69. Kozlov, M. M. et al. Mechanisms shaping cell membranes. *Curr. Opin. Cell Biol.* **29**, 53–60 (2014).
70. Kahraman, O., Langen, R. & Haselwandter, C. A. Directed supramolecular organization of N-BAR proteins through regulation of H0 membrane immersion depth. *Sci. Rep.* **8**, 16383 (2018).
71. Martens, S., Kozlov, M. M. & McMahon, H. T. How synaptotagmin promotes membrane fusion. *Science* **316**, 1205–1208 (2007).
72. Chernomordik, L. Non-bilayer lipids and biological fusion intermediates. *Chem. Phys. Lipids* **81**, 203–213 (1996).
73. Fuller, N. & Rand, R. P. The influence of lysolipids on the spontaneous curvature and bending elasticity of phospholipid membranes. *Biophys. J.* **81**, 243–254 (2001).
74. Fernandes, F. et al. Role of helix 0 of the N-BAR domain in membrane curvature generation. *Biophys. J.* **94**, 3065–3073 (2008).
75. Chen, Z., Zhu, C., Kuo, C. J., Robustelli, J. & Baumgart, T. The N-terminal amphipathic helix of endophilin does not contribute to its molecular curvature generation capacity. *J. Am. Chem. Soc.* **138**, 14616–14622 (2016).
76. Sheetz, M. P. & Singer, S. J. Biological membranes as bilayer couples. A molecular mechanism of drug-erythrocyte interactions. *Proc. Natl Acad. Sci. USA* **71**, 4457–4461 (1974).
77. Hossein, A. & Deserno, M. Spontaneous curvature, differential stress, and bending modulus of asymmetric lipid membranes. *Biophys. J.* **118**, 624–642 (2020).
78. Miettinen, M. S. & Lipowsky, R. Bilayer membranes with frequent flip-flops have tensionless leaflets. *Nano Lett.* **19**, 5011–5016 (2019).
79. Kozlov, M. M. & Helfrich, W. Effects of a cosurfactant on the stretching and bending elasticities of a surfactant monolayer. *Langmuir* **8**, 2792–2797 (2002).

80. Markin, V. S. Lateral organization of membranes and cell shapes. *Biophys. J.* **36**, 1–19 (1981).
81. Fournier, J.-B. Microscopic membrane elasticity and interactions among membrane inclusions: interplay between the shape, dilation, tilt and tilt-difference modes. *Eur. Phys. J. B Condens. Matter Complex. Syst.* **11**, 261–272 (2012).
82. Messa, M. et al. Epsin deficiency impairs endocytosis by stalling the actin-dependent invagination of endocytic clathrin-coated pits. *Elife* **3**, e03311 (2014).
83. Miller, S. E. et al. CALM regulates clathrin-coated vesicle size and maturation by directly sensing and driving membrane curvature. *Dev. Cell* **33**, 163–175 (2015).
84. Busch, D. J. et al. Intrinsically disordered proteins drive membrane curvature. *Nat. Commun.* **6**, 1–11 (2015).
85. Bickel, T., Jeppesen, C. & Marques, C. M. Local entropic effects of polymers grafted to soft interfaces. *Eur. Phys. J. E* **4**, 33–43 (2001).
86. Hiergeist, C. & Lipowsky, R. Elastic properties of polymer-decorated membranes. *J. Phys. II* **6**, 1465–1481 (1996).
87. Hristova, K. & Needham, D. The influence of polymer-grafted lipids on the physical properties of lipid bilayers: a theoretical study. *J. Colloid . Interface Sci.* **168**, 302–314 (1994).
88. Kuo, J. C. H. & Paszek, M. J. Glycocalyx curving the membrane: forces emerging from the cell exterior. *Annu. Rev. Cell Dev. Biol.* **37**, 257–283 (2021).
89. Lipowsky, R. Bending of membranes by anchored polymers. *Europhys. Lett.* **30**, 197 (1995).
90. Marsh, D. Elastic constants of polymer-grafted lipid membranes. *Biophys. J.* **81**, 2154–2162 (2001).
91. Milner, S. T. & Witten, T. A. Bending moduli of polymeric surfactant interfaces. *J. Phys.* **49**, 1951–1962 (1988).
92. Sens, P. & Turner, M. S. Theoretical model for the formation of caveolae and similar membrane invaginations. *Biophys. J.* **86**, 2049–2057 (2004).
93. Shurer, C. R. et al. Physical principles of membrane shape regulation by the glycocalyx. *Cell* **177**, 1757–1770.e1721 (2019).
94. Tsafrir, I., Caspi, Y., Guedeau-Boudeville, M. A., Arzi, T. & Stavans, J. Budding and tubulation in highly oblate vesicles by anchored amphiphilic molecules. *Phys. Rev. Lett.* **91**, 138102 (2003).
95. Lerche, D., Kozlov, M. M. & Markin, V. S. Electrostatic free-energy and spontaneous curvature of spherical charged layered membrane. *Biorheology* **24**, 23–34 (1987).
96. Button, B. et al. A periciliary brush promotes the lung health by separating the mucus layer from airway epithelia. *Science* **337**, 937–941 (2012).
97. Bennett, R. J. et al. Mucin MUC1 is seen in cell surface protrusions together with ezrin in immunoelectron tomography and is concentrated at tips of filopodial protrusions in MCF-7 breast carcinoma cells. *J. Histochem. Cytochem.* **49**, 67–77 (2001).
98. Kesimer, M. et al. Molecular organization of the mucins and glycocalyx underlying mucus transport over mucosal surfaces of the airways. *Mucosal Immunol.* **6**, 379–392 (2012).
99. Fowke, T. M. et al. Hyaluronan synthesis by developing cortical neurons in vitro. *Sci. Rep.* **7**, 1–13 (2017).
100. Zeno, W. F. et al. Molecular mechanisms of membrane curvature sensing by a disordered protein. *J. Am. Chem. Soc.* **141**, 10361–10371 (2019).
101. Zeno, W. F., Snead, W. T., Thatte, A. S. & Stachowiak, J. C. Structured and intrinsically disordered domains within Amphiphysin1 work together to sense and drive membrane curvature. *Soft Matter* **15**, 8706–8717 (2019).
102. Alexander, S. Adsorption of chain molecules with a polar head a-scaling description. *J. Phys.* **38**, 983–987 (1977).
103. Alexander, S. Polymer adsorption on small spheres - scaling approach. *J. Phys.* **38**, 977–981 (1977).
104. de Gennes, P. G. Conformations of polymers attached to an interface. *Macromolecules* **13**, 1069–1075 (1980).
105. Marsh, D., Bartucci, R. & Sportelli, L. Lipid membranes with grafted polymers: physicochemical aspects. *Biochim. Biophys. Acta Biomembr.* **1615**, 33–59 (2003).
106. Banani, S. F., Lee, H. O., Hyman, A. A. & Rosen, M. K. Biomolecular condensates: organizers of cellular biochemistry. *Nat. Rev. Mol. Cell Biol.* **18**, 285–298 (2017).
107. Li, P. et al. Phase transitions in the assembly of multivalent signalling proteins. *Nature* **483**, 336–340 (2012).
108. Yuan, F. et al. Membrane bending by protein phase separation. *Proc. Natl Acad. Sci. USA* https://doi.org/10.1073/PNAS.2017435118 (2021).
109. Simunovic, M., Evergren, E., Callan-Jones, A. & Bassereau, P. Curving cells inside and out: roles of BAR domain proteins in membrane shaping and its cellular implications. *Annu. Rev. Cell Dev. Biol.* **35**, 111–129 (2019).
110. Zhang, Y. et al. Structural insights into membrane remodeling by SNX1. *Proc. Natl Acad. Sci. USA* https://doi.org/10.1073/pnas.2022614118 (2021).
111. Leneva, N., Kovtun, O., Morado, D. R., Briggs, J. A. G. & Owen, D. J. Architecture and mechanism of metazoan retromer:SNX3 tubular coat assembly. *Sci. Adv.* **7**, 1–10 (2021).
112. Johannes, L. The cellular and chemical biology of endocytic trafficking and intracellular delivery — the GL-Lect hypothesis. *Molecules* https://doi.org/10.3390/MOLECULES26113299 (2021).
113. Dodonova, S. O. et al. A structure of the COPI coat and the role of coat proteins in membrane vesicle assembly. *Science* **349**, 195–198 (2015).
114. Bi, X., Corpina, R. A. & Goldberg, J. Structure of the SEC23/24-SAR1 pre-budding complex of the COPII vesicle coat. *Nature* **419**, 271–277 (2002).
115. Kirchhausen, T., Owen, D. & Harrison, S. C. Molecular structure, function, and dynamics of clathrin-mediated membrane traffic. *Cold Spring Harb. Perspect. Biol.* https://doi.org/10.1101/CSHPERSPECT.A016725 (2014).
116. Antonny, B. et al. Membrane fission by dynamin: what we know and what we need to know. *EMBO J.* **35**, 2270–2284 (2016).
117. Caillat, C., Maity, S., Miguet, N., Roos, W. H. & Weissenhorn, W. The role of VPS4 in ESCRT-III polymer remodeling. *Biochem. Soc. Trans.* **47**, 441–448 (2019).
118. Remec Pavlin, M. & Hurley, J. H. The ESCRTs - converging on mechanism. *J. Cell Sci.* https://doi.org/10.1242/jcs.240333 (2020).
119. Sundquist, W. I. & Kräusslich, H. G. HIV-1 assembly, budding, and maturation. *Cold Spring Harb. Perspect. Med.* https://doi.org/10.1101/CSHPERSPECT.A006924 (2012).
120. Frost, A. et al. Structural basis of membrane invagination by F-BAR domains. *Cell* **132**, 807–817 (2008).
121. Yu, H. & Schulten, K. Membrane sculpting by F-BAR domains studied by molecular dynamics simulations. *PLoS Comput. Biol.* **9**, e1002892 (2013).
122. Ling, H. et al. Structure of the Shiga-like toxin I B-pentamer complexed with an analogue of its receptor Gb3. *Biochemistry* **37**, 1777–1788 (1998).
123. Zheng, J. et al. Identification of the binding site for acidic phospholipids on the PH domain of dynamin: implications for stimulation of GTPase activity. *J. Mol. Biol.* **255**, 14–21 (1996).
124. Cremona, O. & De Camilli, P. Phosphoinositides in membrane traffic at the synapse. *J. Cell Sci.* **114**, 1041–1052 (2001).
125. Johannes, L., Wunder, C. & Bassereau, P. Bending "on the rocks" — a cocktail of biophysical modules to build endocytic pathways. *Cold Spring Harb. Perspect. Biol.* **6** https://doi.org/10.1101/CSHPERSPECT.A016741 (2014).
126. Pezeshkian, W. et al. Membrane invagination induced by Shiga toxin B-subunit: from molecular structure to tube formation. *Soft Matter* **12**, 5164–5171 (2016).
127. Mim, C. & Unger, V. M. Membrane curvature and its generation by BAR proteins. *Trends Biochem. Sci.* **37**, 526–533 (2012).
128. Bonifacino, J. S. & Lippincott-Schwartz, J. Coat proteins: shaping membrane transport. *Nat. Rev. Mol. Cell Biol.* **4**, 409–414 (2003).
129. Mettlen, M., Chen., P.-H., Srinivasan, S., Danuser, G. & Schmid, S. L. Regulation of clathrin-mediated endocytosis. *Annu. Rev. Biochem.* **87**, 871–896 (2018).
130. Fotin, A. et al. Molecular model for a complete clathrin lattice from electron cryomicroscopy. *Nature* **432**, 573–579 (2004).
131. Sochacki, K. A. & Taraska, J. W. From flat to curved clathrin: controlling a plastic ratchet. *Trends Cell Biol.* **29**, 241–256 (2019).
132. Kaneseki, T. & Kadota, K. The "vesicle in a basket". *J. Cell Biol.* **42**, 202–220 (1969).
133. Roth, T. F. & Porter, K. R. Yolk protein uptake in the oocyte of the mosquito *Aedes aegypti* L. *J. Cell Biol.* **20**, 313–332 (1964).
134. Taylor, M. J., Perrais, D. & Merrifield, C. J. A high precision survey of the molecular dynamics of mammalian clathrin-mediated endocytosis. *PLoS Biol.* **9**, e1000604 (2011).
135. Merrifield, C. J., Feldman, M. E., Wan, L. & Almers, W. Imaging actin and dynamin recruitment during invagination of single clathrin-coated pits. *Nat. Cell Biol.* **4**, 691–698 (2002).
136. Gaidarov, I., Santini, F., Warren, R. A. & Keen, J. H. Spatial control of coated-pit dynamics in living cells. *Nat. Cell Biol.* **1**, 1–7 (1999).
137. Kirchhausen, T. Imaging endocytic clathrin structures in living cells. *Trends Cell Biol.* **19**, 596–605 (2009).
138. Kaksonen, M., Toret, C. P. & Drubin, D. G. A modular design for the clathrin- and actin-mediated endocytosis machinery. *Cell* **123**, 305–320 (2005).
139. Taylor, M. J., Lampe, M. & Merrifield, C. J. A feedback loop between dynamin and actin recruitment during clathrin-mediated endocytosis. *PLoS Biol.* **10**, e1001302 (2012).
140. Li, D. et al. Advanced imaging. Extended-resolution structured illumination imaging of endocytic and cytoskeletal dynamics. *Science* **349**, aab3500 (2015).
141. Chen, Z. & Schmid, S. L. Evolving models for assembling and shaping clathrin-coated pits. *J. Cell Biol.* https://doi.org/10.1083/JCB.202005126 (2020).
142. Heuser, J. & Keen, J. Deep-etch visualization of proteins involved in clathrin assembly. *J. Cell Biol.* **107**, 877–886 (1988).
143. Sochacki, K. A. et al. The structure and spontaneous curvature of clathrin lattices at the plasma membrane. *Dev. Cell* **56**, 1131–1146.e1133 (2021).
144. Kovtun, O., Dickson, V. K., Kelly, B. T., Owen, D. J. & Briggs, J. A. G. Architecture of the AP2/clathrin coat on the membranes of clathrin-coated vesicles. *Sci. Adv.* **6**, 1–10 (2020).
145. Posor, Y. et al. Spatiotemporal control of endocytosis by phosphatidylinositol-3,4-bisphosphate. *Nature* **499**, 233–237 (2013).
146. Park, R. J. et al. Dynamin triple knockout cells reveal off target effects of commonly used dynamin inhibitors. *J. Cell Sci.* **126**, 5305–5312 (2013).
147. Cocucci, E., Aguet, F., Boulant, S. & Kirchhausen, T. The first five seconds in the life of a clathrin-coated pit. *Cell* **150**, 495–507 (2012).
148. Ma, L. et al. Transient Fcho1/2Eps15/RAP-2 nanoclusters prime the AP-2 clathrin adaptor for cargo binding. *Dev. Cell* **37**, 428–443 (2016).
149. Traub, L. M. A nanobody-based molecular toolkit provides new mechanistic insight into clathrin-coat initiation. *Elife* https://doi.org/10.7554/eLife.41768 (2019).
150. Henne, W. M. et al. FCHo proteins are nucleators of clathrin-mediated endocytosis. *Science* **328**, 1281–1284 (2010).
151. Kozak, M. & Kaksonen, M. Condensation of Ede1 promotes the initiation of endocytosis. *Elife* https://doi.org/10.7554/eLife.72865 (2022).
152. Day, K. J. et al. Liquid-like protein interactions catalyse assembly of endocytic vesicles. *Nat. Cell Biol.* **23**, 366–376 (2021).
153. Sochacki, K. A., Dickey, A. M., Strub, M. P. & Taraska, J. W. Endocytic proteins are partitioned at the edge of the clathrin lattice in mammalian cells. *Nat. Cell Biol.* **19**, 352–361 (2017).
154. Haucke, V. & Kozlov, M. M. Membrane remodeling in clathrin-mediated endocytosis. *J. Cell Sci.* **131**, jcs216812 (2018).
155. Teyra, J. et al. Comprehensive analysis of the human SH3 domain family reveals a wide variety of non-canonical specificities. *Structure* **25**, 1598–1610.e1593 (2017).
156. Matthaeus, C. & Taraska, J. W. Energy and dynamics of caveolae trafficking. *Front. Cell Dev. Biol.* **8**, 614472 (2020).
157. Bucher, D. et al. Clathrin-adaptor ratio and membrane tension regulate the flat-to-curved transition of the clathrin coat during endocytosis. *Nat. Commun.* **9**, 1–13 (2018).
158. Dambournet, D. et al. Genome-edited human stem cells expressing fluorescently labeled endocytic markers allow quantitative analysis of clathrin-mediated endocytosis during differentiation. *J. Cell Biol.* **217**, 3301–3311 (2018).
159. Heuser, J. Effects of cytoplasmic acidification on clathrin lattice morphology. *J. Cell Biol.* **108**, 401–411 (1989).
160. Tagiltsev, G., Haselwandter, C. A. & Scheuring, S. Nanodissected elastically loaded clathrin lattices relax to increased curvature. *Sci. Adv.* https://doi.org/10.1126/sciadv.abg9934 (2021).
161. Zeno, W. F. et al. Clathrin senses membrane curvature. *Biophys. J.* **120**, 818–828 (2021).
162. Dannhauser, P. N. & Ungewickell, E. J. Reconstitution of clathrin-coated bud and vesicle formation with minimal components. *Nat. Cell Biol.* **14**, 634 (2012).
163. Avinoam, O., Schorb, M., Beese, C. J., Briggs, J. A. & Kaksonen, M. Endocytic sites mature by continuous bending and remodeling of the clathrin coat. *Science* **348**, 1369–1372 (2015).

164. Scott, B. L. et al. Membrane bending occurs at all stages of clathrin-coat assembly and defines endocytic dynamics. *Nat. Commun.* **9**, 1–9 (2018).
165. Nawara, T. J. et al. Imaging vesicle formation dynamics supports the flexible model of clathrin-mediated endocytosis. *Nat. Commun.* **13**, 1732 (2022).
166. Grove, J. et al. Flat clathrin lattices: stable features of the plasma membrane. *Mol. Biol. Cell* **25**, 3581–3594 (2014).
167. Nossal, R. Energetics of clathrin basket assembly. *Traffic* **2**, 138–147 (2001).
168. Alfonzo-Mendez, M. A., Sochacki, K. A., Strub, M. P. & Taraska, J. W. Dual clathrin and integrin signaling systems regulate growth factor receptor activation. *Nat. Commun.* **13**, 905 (2022).
169. Mund, M. et al. Systematic nanoscale analysis of endocytosis links efficient vesicle formation to patterned actin nucleation. *Cell* **174**, 884–896 e817 (2018).
170. Palade, G. E. Fine structure of blood capillaries. *J. Appl. Phys.* **24**, 1424–1424 (1953).
171. Yamada, E. The fine structure of the gall bladder epithelium of the mouse. *J. Biophys. Biochem. Cytol.* **1**, 445–458 (1955).
172. Sinha, B. et al. Cells respond to mechanical stress by rapid disassembly of caveolae. *Cell* **144**, 402–413 (2011).
173. Parton, R. G. & del Pozo, M. A. Caveolae as plasma membrane sensors, protectors and organizers. *Nat. Rev. Mol. Cell Biol.* **14**, 98–112 (2013).
174. Gervasio, O. L., Phillips, W. D., Cole, L. & Allen, D. G. Caveolae respond to cell stretch and contribute to stretch-induced signaling. *J. Cell Sci.* **124**, 3581–3590 (2011).
175. Zhou, Y. et al. Caveolin-1 and cavin1 act synergistically to generate a unique lipid environment in caveolae. *J. Cell Biol.* https://doi.org/10.1083/jcb.202005138 (2021).
176. Han, B., Copeland, C. A., Tiwari, A. & Kenworthy, A. K. Assembly and turnover of caveolae: what do we really know? *Front. Cell Dev. Biol.* **4**, 68 (2016).
177. Feron, O., Michel, J. B., Sase, K. & Michel, T. Dynamic regulation of endothelial nitric oxide synthase: complementary roles of dual acylation and caveolin interactions. *Biochemistry* **37**, 193–200 (1998).
178. Stan, R. V., Kubitza, M. & Palade, G. E. PV-1 is a component of the fenestral and stomatal diaphragms in fenestrated endothelia. *Proc. Natl Acad. Sci. USA* **96**, 13203–13207 (1999).
179. Rothberg, K. G. et al. Caveolin, a protein component of caveolae membrane coats. *Cell* **68**, 673–682 (1992).
180. Cohen, A. W., Hnasko, R., Schubert, W. & Lisanti, M. P. Role of caveolae and caveolins in health and disease. *Physiol. Rev.* **84**, 1341–1379 (2004).
181. Hayer, A., Stoeber, M., Bissig, C. & Helenius, A. Biogenesis of caveolae: stepwise assembly of large caveolin and cavin complexes. *Traffic* **11**, 361–382 (2010).
182. Walser, P. J. et al. Constitutive formation of caveolae in a bacterium. *Cell* **150**, 752–763 (2012).
183. Porta, J. C. et al. The building blocks of caveolae, revealed. *Biophys. J.* **121**, 2–2 (2022).
184. Han, B. et al. Structure and assembly of CAV1 8S complexes revealed by single particle electron microscopy. *Sci. Adv.* https://doi.org/10.1126/sciadv.abc6185 (2020).
185. Tillu, V. A. et al. Cavin1 intrinsically disordered domains are essential for fuzzy electrostatic interactions and caveola formation. *Nat. Commun.* **12**, 931 (2021).
186. Zimnicka, A. M. et al. Src-dependent phosphorylation of caveolin-1 Tyr-14 promotes swelling and release of caveolae. *Mol. Biol. Cell* **27**, 2090–2106 (2016).
187. Hansen, C. G., Howard, G. & Nichols, B. J. Pacsin 2 is recruited to caveolae and functions in caveolar biogenesis. *J. Cell Sci.* **124**, 2777–2785 (2011).
188. Koch, D., Westermann, M., Kessels, M. M. & Qualmann, B. Ultrastructural freeze-fracture immunolabeling identifies plasma membrane-localized syndapin II as a crucial factor in shaping caveolae. *Histochem. Cell Biol.* **138**, 215–230 (2012).
189. Gomez-Navarro, N. & Miller, E. A. COP-coated vesicles. *Curr. Biol.* **26**, R54–R57 (2016).
190. Bethune, J. & Wieland, F. T. Assembly of COPI and COPII vesicular coat proteins on membranes. *Annu. Rev. Biophys.* **47**, 63–83 (2018).
191. Hughes, H. & Stephens, D. J. Assembly, organization, and function of the COPII coat. *Histochem. Cell Biol.* **129**, 129–151 (2008).
192. Hammond, A. T. & Glick, B. S. Dynamics of transitional endoplasmic reticulum sites in vertebrate cells. *Mol. Biol. Cell* **11**, 3013–3030 (2000).
193. Yu, X., Breitman, M. & Goldberg, J. A structure-based mechanism for ARF1-dependent recruitment of coatomer to membranes. *Cell* **148**, 530–542 (2012).
194. Faini, M. et al. The structures of COPI-coated vesicles reveal alternate coatomer conformations and interactions. *Science* **336**, 1451–1454 (2012).
195. Dodonova, S. O. et al. 9A structure of the COPI coat reveals that the ARF1 GTPase occupies two contrasting molecular environments. *Elife* https://doi.org/10.7554/eLife.26691 (2017).
196. Hariri, H., Bhattacharya, N., Johnson, K., Noble, A. J. & Stagg, S. M. Insights into the mechanisms of membrane curvature and vesicle scission by the small GTPase SAR1 in the early secretory pathway. *J. Mol. Biol.* **426**, 3811–3826 (2014).
197. Beck, R. et al. Membrane curvature induced by ARF1-GTP is essential for vesicle formation. *Proc. Natl Acad. Sci. USA* **105**, 11731–11736 (2008).
198. Beck, R. et al. Coatomer and dimeric ADP ribosylation factor 1 promote distinct steps in membrane scission. *J. Cell Biol.* **194**, 765–777 (2011).
199. Boucrot, E. et al. Membrane fission is promoted by insertion of amphipathic helices and is restricted by crescent BAR domains. *Cell* **149**, 124–136 (2012).
200. Kroppen, B. et al. Cooperativity of membrane-protein and protein–protein interactions control membrane remodeling by epsin 1 and affects clathrin-mediated endocytosis. *Cell. Mol. Life Sci.* **78**, 2355–2370 (2021).
201. Tarasenko, D. et al. The MICOS component Mic60 displays a conserved membrane-bending activity that is necessary for normal cristae morphology. *J. Cell Biol.* **216**, 889–899 (2017).
202. Yoon, Y. et al. Molecular basis of the potent membrane-remodeling activity of the epsin 1 N-terminal homology domain. *J. Biol. Chem.* **285**, 531–540 (2010).
203. Braun, A. R., Lacy, M. M., Ducas, V. C., Rhoades, E. & Sachs, J. N. α-Synuclein's uniquely long amphipathic helix enhances its membrane binding and remodeling capacity. *J. Membr. Biol.* **250**, 183–193 (2017).
204. Hoover, B. M. et al. Membrane remodeling and stimulation of aggregation following α-synuclein adsorption to phosphotidylserine vesicles. *J. Phys. Chem. B* **125**, 1582–1594 (2021).
205. Mizuno, N. et al. Remodeling of lipid vesicles into cylindrical micelles by α-synuclein in an extended α-helical conformation. *J. Biol. Chem.* **287**, 29301–29311 (2012).
206. Varkey, J. et al. α-synuclein oligomers with broken helical conformation form lipoprotein nanoparticles. *J. Biol. Chem.* **288**, 17620–17630 (2013).
207. Westphal, C. H. & Chandra, S. S. Monomeric synucleins generate membrane curvature. *J. Biol. Chem.* **288**, 1829–1840 (2013).
208. Powers, R. E., Wang, S., Liu, T. Y. & Rapoport, T. A. Reconstitution of the tubular endoplasmic reticulum network with purified components. *Nature* **543**, 257–260 (2017).
209. Opaliński, Ł., Kiel, J. A. K. W., Williams, C., Veenhuis, M. & Klei, I. J. V. D. Membrane curvature during peroxisome fission requires Pex11. *EMBO J.* **30**, 5–16 (2011).
210. Su, J. et al. The N-terminal amphipathic helix of Pex11p self-interacts to induce membrane remodelling during peroxisome fission. *Biochim. Biophys. Acta Biomembr.* **1860**, 1292–1300 (2018).
211. Bielli, A. et al. Regulation of Sar1 NH 2 terminus by GTP binding and hydrolysis promotes membrane deformation to control COPII vesicle fission. *J. Cell Biol.* **171**, 919–924 (2005).
212. Lee, M. C. S. et al. Sar1p N-terminal helix initiates membrane curvature and completes the fission of a COPII vesicle. *Cell* **122**, 605–617 (2005).
213. Krauss, M. et al. Arf1-GTP-induced tubule formation suggests a function of arf family proteins in curvature acquisition at sites of vesicle budding. *J. Biol. Chem.* **283**, 27717–27723 (2008).
214. Lundmark, R. et al. Arf family GTP loading is activated by, and generates, positive membrane curvature. *Biochem. J.* **414**, 189–194 (2008).
215. Martyna, A. et al. Membrane remodeling by the M2 amphipathic helix drives influenza virus membrane scission. *Sci. Rep.* https://doi.org/10.1038/SREP44695 (2017).
216. Farsad, K. et al. Generation of high curvature membranes mediated by direct endophilin bilayer interactions. *J. Cell Biol.* **155**, 193–200 (2001).
217. Masuda, M. et al. Endophilin BAR domain drives membrane curvature by two newly identified structure-based mechanisms. *EMBO J.* **25**, 2889–2897 (2006).
218. Peter, B. J. et al. BAR domains as sensors of membrane curvature: the amphiphysin BAR structure. *Science* **303**, 495–499 (2004).
219. Takei, K., Slepnev, V. I., Haucke, V. & De Camilli, P. Functional partnership between amphiphysin and dynamin in clathrin-mediated endocytosis. *Nat. Cell Biol.* **1**, 33 (1999).
220. Hui, E., Bai, J. & Chapman, E. R. Ca^{2+}-triggered simultaneous membrane penetration of the tandem C2-domains of synaptotagmin I. *Biophys. J.* **91**, 1767–1777 (2006).
221. Groffen, A. J. et al. Doc2b is a high-affinity Ca^{2+} sensor for spontaneous neurotransmitter release. *Science* **327**, 1614–1618 (2010).
222. Sorkin, R. et al. Synaptotagmin-1 and Doc2b exhibit distinct membrane-remodeling mechanisms. *Biophys. J.* **118**, 643–656 (2020).
223. Helfrich, W. Elastic properties of lipid bilayers: theory and possible experiments. *Z. Naturforsch. Sect. C.* **28**, 693–703 (1973).
224. Doktorova, M., Harries, D. & Khelashvili, G. Determination of bending rigidity and tilt modulus of lipid membranes from real-space fluctuation analysis of molecular dynamics simulations. *Phys. Chem. Chem. Phys.* **19**, 16806–16818 (2017).
225. May, S., Kozlovsky, Y., Ben-Shaul, A. & Kozlov, M. M. Tilt modulus of a lipid monolayer. *Eur. Phys. J. E* **14**, 299–308 (2004).
226. Nagle, J. F., Jablin, M. S., Tristram-Nagle, S. & Akabori, K. What are the true values of the bending modulus of simple lipid bilayers? *Chem. Phys. Lipids* **185**, 3–10 (2015).
227. Siegel, D. P. & Kozlov, M. M. The gaussian curvature elastic modulus of N-monomethylated dioleoylphosphatidylethanolamine: relevance to membrane fusion and lipid phase behavior. *Biophys. J.* **87**, 366–374 (2004).
228. Kozlovsky, Y. & Kozlov, M. M. Membrane fission: model for intermediate structures. *Biophys. J.* **85**, 85–96 (2003).
229. Kozlovsky, Y. & Kozlov, M. M. Stalk model of membrane fusion: solution of energy crisis. *Biophys. J.* **82**, 882–895 (2002).
230. Dimova, R. Recent developments in the field of bending rigidity measurements on membranes. *Adv. Colloid Interface Sci.* **208**, 225–234 (2014).
231. Bickel, T., Marques, C. & Jeppesen, C. Pressure patches for membranes: the induced pinch of a grafted polymer. *Phys. Rev. E* **62**, 1124 (2000).
232. Breidenich, M., Netz, R. R. & Lipowsky, R. The shape of polymer-decorated membranes. *Europhys. Lett.* **49**, 431 (2000).
233. Blondeau, F. et al. Tandem MS analysis of brain clathrin-coated vesicles reveals their critical involvement in synaptic vesicle recycling. *Proc. Natl Acad. Sci. USA* **101**, 3833–3838 (2004).

Acknowledgements
M.M.K. is supported by SFB 958 "Scaffolding of Membranes" (Germany) and Singapore–Israel (NRF-ISF) research grant 3292/19. J.W.T is supported by the Intramural Research Program of the US National Heart, Lung, and Blood Institute, National Institutes of Health. The authors apologize to the many authors whose work could not to be specifically cited in this Review due to space constraints and the long, deep and rich history of this growing and innovative field.

Author contributions
The authors contributed equally to all aspects of the article.

Competing interests
The authors declare no competing interests.

Peer review information
Nature Reviews Molecular Cell Biology thanks Patricia Bassereau, Tobias Baumgart, who co-reviewed with Samsuzzoha Mondal and Rumiana Dimova, who co-reviewed with Jan Steinkühler for their contribution to the peer review of this work.

Publisher's note
Springer Nature remains neutral with regard to jurisdictional claims in published maps and institutional affiliations.

Springer Nature or its licensor holds exclusive rights to this article under a publishing agreement with the author(s) or other rightsholder(s); author self-archiving of the accepted manuscript version of this article is solely governed by the terms of such publishing agreement and applicable law.

Supplementary information
The online version contains supplementary material available at https://doi.org/10.1038/s41580-022-00511-9.

This is a U.S. Government work and not under copyright protection in the US; foreign copyright protection may apply 2022